The Glutamate Transporter Subtypes EAAT4 and EAATs 1-3 Transport Glutamate with Dramatically Different Kinetics and Voltage Dependence but Share a Common Uptake Mechanism

Carsten Mim,[1,2] Poonam Balani,[3] Thomas Rauen,[4] and Christof Grewer[1]

[1]University of Miami School of Medicine, Miami, FL 33136
[2]Max-Planck-Institut für Biophysik, D-60438 Frankfurt, Germany
[3]Westfälische-Wilhelms-Universität Münster, D-48149 Münster, Germany
[4]Universität Osnabrück, Fachbereich Biologie/Chemie, Abteilung Biophysik, D-49034 Osnabrück, Germany

Here, we report the application of glutamate concentration jumps and voltage jumps to determine the kinetics of rapid reaction steps of excitatory amino acid transporter subtype 4 (EAAT4) with a 100-μs time resolution. EAAT4 was expressed in HEK293 cells, and the electrogenic transport and anion currents were measured using the patch-clamp method. At steady state, EAAT4 was activated by glutamate and Na^+ with high affinities of 0.6 μM and 8.4 mM, respectively, and showed kinetics consistent with sequential binding of Na^+-glutamate-Na^+. The steady-state cycle time of EAAT4 was estimated to be >300 ms (at −90 mV). Applying step changes to the transmembrane potential, V_m, of EAAT4-expressing cells resulted in the generation of transient anion currents (decaying with a τ of ∼15 ms), indicating inhibition of steady-state EAAT4 activity at negative voltages (<−40 mV) and activation at positive V_m (>0 mV). A similar inhibitory effect at $V_m < 0$ mV was seen when the electrogenic glutamate transport current was monitored, resulting in a bell-shaped I-V_m curve. Jumping the glutamate concentration to 100 μM generated biphasic, saturable transient transport and anion currents ($K_m \sim 5$ μM) that decayed within 100 ms, indicating the existence of two separate electrogenic reaction steps. The fast electrogenic reaction was assigned to Na^+ binding to EAAT4, whereas the second reaction is most likely associated with glutamate translocation. Together, these results suggest that glutamate uptake of EAAT4 is based on the same molecular mechanism as transport by the subtypes EAATs 1–3, but that its kinetics and voltage dependence are dramatically different from the other subtypes. EAAT4 kinetics appear to be optimized for high affinity binding of glutamate, but not rapid turnover. Therefore, we propose that EAAT4 is a high-affinity/low-capacity transport system, supplementing low-affinity/high-capacity synaptic glutamate uptake by the other subtypes.

The Journal of General Physiology

INTRODUCTION

In the mammalian brain the excitatory neurotransmitter glutamate is removed from the extracellular space by active uptake into glial cells and neurons. This uptake is mediated by high-affinity transporters that are expressed at and around glutamatergic synapses in high density (Lehre and Danbolt, 1998; Danbolt, 2001). Glutamate transport is coupled to cotransport of three Na^+ ions and 1 H^+, and countertransport of 1 K^+ (Zerangue and Kavanaugh, 1996; Levy et al., 1998). It is believed that this stoichiometry enables glutamate transporters to keep the steady-state extracellular concentration of glutamate below the micromolar range (Zerangue and Kavanaugh, 1996), which is essential for normal functioning of the nervous system.

Five glutamate transporter subtypes have been cloned that are expressed either in glial cells (excitatory amino acid transporters [EAATs] 1–2, also named glutamate-aspartate transporter [GLAST] [Storck et al., 1992], and glutamate transporter 1 [GLT-1] [Pines et al., 1992]), or in neurons (EAAT3, also named excitatory amino acid carrier 1 [EAAC1] [Kanai and Hediger, 1992], and EAATs 4–5 [Fairman et al., 1995; Arriza et al., 1997]). The electrogenic properties of the subtypes EAATs 1–3 have been extensively studied (for reviews see Danbolt, 2001; Grewer and Rauen, 2005). It was found that these glutamate transporter subtypes not only catalyze Na^+-coupled electrogenic glutamate transport across the membrane, but they also mediate glutamate-dependent transmembrane anion fluxes that are specific for hydrophobic anions (Picaud et al., 1995; Wadiche et al., 1995a; Eliasof and Jahr, 1996). Thus, glutamate-induced EAAT currents consist of two components: the transport current generated by the electrogenic, coupled movement of glutamate and the co- and counter-transported ions across the membrane, and the anion current generated by uncoupled,

Correspondence to Christof Grewer: cgrewer@med.miami.edu

Abbreviations used in this paper: CMV, cytomegalo virus; EAAC1, excitatory amino acid carrier 1; EAAT, excitatory amino acid transporter; GHK, Goldman-Hodgkin-Katz; HEK, human embryonic kidney; MeS, methanesulfonate; MNI, 4-methoxy-7-nitroindyl; TBOA, dl-*threo*-β-benzyloxyaspartate.

glutamate-gated transmembrane anion flow. It has been suggested that the physiological function of anion influx is to counterbalance the influx of positive charge during glutamate transport and, thus, to prevent the cell from depolarizing (Sonders and Amara, 1996). Whereas the transport current catalyzed by the subtypes EAATs 1–3 is of substantial magnitude and easily measured in human embryonic kidney (HEK)-293 cells (Grewer et al., 2001; Watzke et al., 2001) and *Xenopus* oocytes (Wadiche et al., 1995b), substrate application to EAAT4-expressing oocytes results in very small inward transport current in the range of −10 nA (Mitrovic et al., 2001). Currents carried by EAAT4, therefore, have been mainly attributed to the anion current component (Fairman et al., 1995; Lin et al., 1998). Because of the small transport currents it is likely that the turnover number of EAAT4 is reduced compared with that of subtypes 1–3. However, there are no reports available on the direct measurement of the turnover rate of EAAT4.

For the glutamate transporter subtypes 1–3 turnover rates have been determined by using presteady-state kinetic methods (Wadiche and Kavanaugh, 1998; Watzke et al., 2001; Bergles et al., 2002). The application of these methods has also revealed a wealth of information on the kinetics and electrogenicity of partial reactions in the transport cycle. In particular, it was determined that partial reactions associated with the glutamate translocation branch of the transport cycle are electrogenic and occur on a time scale of milliseconds, which is fast compared with the turnover of these transporters (Grewer et al., 2000, 2001; Otis and Kavanaugh, 2000; Watzke et al., 2001). Furthermore, based on presteady-state kinetics it was proposed that the rate limiting step in the transport cycle is associated with the potassium-induced relocation reaction of the empty transporter (Grewer et al., 2000). For EAAT4, no such presteady-state experiments have been performed with the recombinantly expressed transporter. However, in two reports presteady-state kinetics of native glutamate transporters expressed in cerebellar Purkinje neurons were determined (Otis and Jahr, 1998; Auger and Attwell, 2000). These native transporters were assumed to be EAAT4. However, EAAT3 is also expressed in Purkinje neurons (Furuta et al., 1997). The general properties and kinetics of the presteady-state currents in these neurons and the turnover rates of these native transporters (14–17 s^{-1}) were very similar to those previously reported for the subtypes 1–3 (Wadiche et al., 1995b; Grewer et al., 2000, 2001; Otis and Kavanaugh, 2000; Watzke et al., 2001). These results are in discrepancy with the steady-state data obtained from recombinantly expressed EAAT4 (Fairman et al., 1995; Mitrovic et al., 2001).

Here, we determined the presteady-state kinetics of EAAT4 expressed in HEK293 cells by recording anion and transport currents induced by applying submillisecond concentration jumps of glutamate to the transporter. Our results showed that EAAT4 presteady-state kinetics and steady-state turnover are significantly slower than those of EAATs 1–3 expressed in the same cell line. In contrast, the apparent and intrinsic affinities of EAAT4 for glutamate are 10-fold higher than those of EAATs 1–3. Furthermore, glutamate transport by EAAT4 has a unique voltage dependence, leading to inhibition at negative membrane potentials close to the resting potential of neurons, while glutamate is bound even more strongly under these conditions. Together, these results suggest that EAAT4 is a high-affinity, low-capacity transport system for glutamate that is kinetically optimized for tight glutamate binding, but not fast uptake. In the brain, EAAT4 function is likely to be important for removal of residual extracellular glutamate at low concentrations that escaped uptake by the low-affinity, high-capacity transporters EAATs 1–3.

MATERIALS AND METHODS

Cell Culture and Molecular Biology

Cell culturing (HEK293, American Type Culture Collection (ATCC) no. CRL 1573) and transfections were performed using the calcium phosphate method as previously described (Watzke et al., 2001), or with the Effectene method (QIAGEN) according to the manufacturer's protocol. EAAT4 cDNA in a cytomegalo virus (CMV) promotor–containing plasmid was provided by S. Amara (University of Pittsburgh School of Medicine, Pittsburgh, PA). In brief, subconfluent human embryonic kidney cell (HEK293, ATCC no. CRL 1573) cultures were transiently transfected either with pCMV-EAAT4 or with pBK-CMV (mock transfection) (40 $\mu g/5 \times 10^6$ cells) by calcium phosphate–mediated transfection as previously described (Watzke et al., 2001). At 2 d post-transfection, cell cultures or membrane vesicles were prepared from the two sets of transfected cells for uptake of radiolabeled substrate, immunoblot analysis, immuncytochemistry, and electrophysiology as previously described (Grewer et al., 2000). For immunoblot analysis or immunocytochemistry, antibodies directed against the COOH-terminal region of EAAT4 (rabbit anti-glutamate transporter EAAT4; BioTrend) were used at a concentration of 1 $\mu g/ml$ and 2 $\mu g/ml$, respectively. For direct comparisons of EAAT4 function with that of other transporter subtypes, we have used rat EAAC1. This transporter has 93% sequence similarity with human EAAT3.

Whole-cell Current Recording

Glutamate-induced currents were measured in the whole-cell current-recording configuration at room temperature. Whole-cell currents were recorded with an Adams & List EPC7 amplifier under voltage-clamp conditions. The resistance of the recording electrode was 2–3 MΩ; the series resistance 4–6 MΩ. SCN^- was in the intracellular or extracellular solutions because it enhances glutamate transporter–induced currents (Wadiche et al., 1995a). For determining the anion current induced by SCN^- outflow, the intracellular and extracellular solutions contained 130 mM KSCN, 1 mM $MgCl_2$, 10 mM EGTA, 10 mM HEPES (pH 7.3), and 140 mM NaCl, 2 mM $MgCl_2$, 2 mM $CaCl_2$, 10 mM HEPES (pH 7.3), respectively. For the measurements of anion current induced by anion inflow, external NaCl was substituted by NaSCN

and the pipette solution contained KCl instead of KSCN. To obtain transport currents, intracellular KSCN was substituted by potassium-methanesulfonate (KMeS) and extracellular NaCl was replaced by NaMeS.

Laser-pulse Photolysis and Rapid Solution Exchange

Laser-pulse photolysis experiments were performed as previously described (Watzke et al., 2001). In brief, glutamate, α-carboxy-o-nitrobenzyl (αCNB)-caged glutamate (Invitrogen) or 4-methoxy-7-nitroindyl (MNI)-caged glutamate (TOCRIS) was applied by means of a small quartz tube (350 μM diameter) to the cells with a velocity of 5 cm/s and a time resolution of 20–30 ms (10–90% rise time with whole cells). In the majority of the experiments, MNI-glutamate was used as caged glutamate precursor because of its high stability in aqueous solutions (Canepari et al., 2001; Maier et al., 2005). We verified that MNI has the same characteristics as CNB with respect to the glutamate-elicited EAAT4 current signals (not depicted). Photolysis of caged glutamate was initiated with a light flash (340 nm, 15 ns, excimer laser pumped dye laser; Lambda Physik), which was delivered to the cell with an optical fiber (350 μm diameter). Laser energies were varied in the range of 50–450 mJ/cm^2 with neutral density filters. To estimate the concentration of photolytically released glutamate a standard glutamate concentration of 100 μM was applied to the cell by rapid perfusion before and after photolysis experiments and the steady-state current amplitude was used to calculate the free glutamate concentration from the dose–response curve (Watzke et al., 2001).

Data were low pass-filtered at 1–20 kHz, digitized with a sampling rate of 5–50 kHz, and recorded using the pClamp8 software (Axon Instruments). To perform voltage-dependent current recordings, we used two types of protocols, a voltage ramp protocol and a voltage jump protocol. Data were analyzed using the Origin (MicroCal) software. Kinetic modeling was performed with the Scientist program (Micromath).

Modeling

We have used a simplified four-step sequential transport model to explain the experimental data. This model includes (a) a reversible glutamate binding reaction to the transporter on the extracellular side, characterized by the rate constants k_{+1} and k_{-1}. Binding and dissociation of glutamate were assumed to be modulated by the preceding and subsequent Na^+ binding steps, which were assumed to be in rapid preequilibrium with respect to glutamate binding. Thus, the overall reaction from T to $\overline{N_2TG}$ reduces to an apparent one-step process. (b) A reversible glutamate translocation reaction (rate constants k_t and k_{-t}). Glutamate translocation was assumed to be reversible for modeling of the exchange mode. In this mode, high intracellular concentrations of glutamate and Na^+ were used that saturate their intracellular binding sites. Thus, glutamate and Na^+ are prevented to dissociate to the cytoplasm, locking the transporter in states $\overline{N_2TG}$ and $\overline{N_2T'G}$ (shaded area in Scheme 1). The model also includes two under forward transport conditions quasi-irreversible transport steps. (c) A reaction characterized by k_2 which could be linked to any of the intracellular substrate dissociation steps, such as glutamate dissociation (see Scheme 1) or Na^+ dissociation. This step was assumed to be quasi-irreversible because the cytoplasmic Na^+ and glutamate concentrations under forward transport conditions should be nominally zero. Therefore, Na^+ and glutamate are prevented from associating to the transporter after dissociation has taken place. (d) The K^+-driven relocation reaction characterized by the rate constant k_r, which might be either the K^+ translocation reaction, association with intracellular K^+, or dissociation of extracellular K^+. This step was also assumed to be quasi-irreversible because the extracellular [K^+] was zero, thus preventing reassociation of extracellular K^+ with EAAT4 and driving the transporter into state T (Scheme 1).

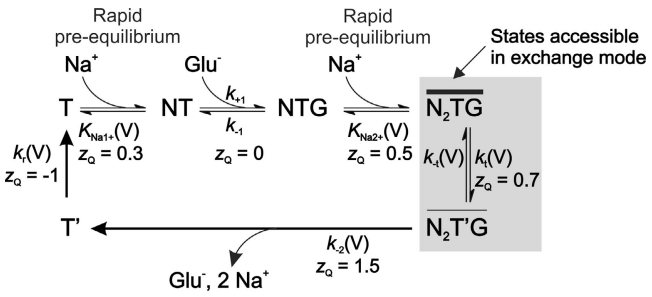

Scheme 1. Pseudo four-state model used for kinetic modeling of EAAT4 anion currents. The detailed kinetic parameters used for modeling are listed in table 1.

Although glutamate binding in step 1 was assumed to be electroneutral, this step is associated with an apparent valence of +0.8, due to the rapid electrogenic Na^+ binding steps preceding and following glutamate binding. Steps 2, 3, and 4 were assumed to be electrogenic with an apparent valence, z_Q, of 0.7 and +1.5, and −1.0, respectively (see Scheme 1). These apparent valencies were selected such that the overall charge moved during one transport cycle was +2.0, according to the stoichiometry determined for EAATs 2 and 3 of 3 Na^+, 1 H^+, and 1 Glu^- cotransported for each K^+ counter-transported (Zerangue and Kavanaugh, 1996; Levy et al., 1998). Based on our data, there was no indication that the EAAT4 stoichiometry is different from that of the subtypes 2 and 3. The values of the apparent valencies given above result in simulations that fitted the experimental data best (see Fig. 10). For example, when z_Q for k_r deviated strongly from −1.0, the current voltage relationship of the steady-state anion and transport currents under forward transport conditions (Fig. 3 B, blue circles; Fig. 3 C) could not be well described. The value of the apparent valencies that is the least defined is that of +1.5 for step 3. Variation of this value from +0.5 to +2 did not result in a significant change in the simulations. This is, of course, expected, since k_{-2} is the fastest reaction step in this cycle, and, thus, far from being rate limiting for the steady-state current or any of the presteady-state phases observed.

The state of main interest is the main anion conducting state, $\overline{N_2TG}$, although a small anion conductance was also assumed for the inward-facing conformation $\overline{N_2T'G}$ (unitary current carried by $\overline{N_2T'G}$ was assumed to be 30% of that carried by $\overline{N_2TG}$). The reason behind this assumption was the voltage dependence of steady-state anion current obtained in the exchange mode (Fig. 3 B). If state $\overline{N_2T'G}$ was not anion conducting at all, this current–voltage relationship should show a maximum and current should decline with increasingly negative membrane potentials, because the transporter would be trapped in state $\overline{N_2T'G}$ under these conditions. In contrast, if $\overline{N_2T'G}$ would have the same anion conductance as $\overline{N_2TG}$ the anion current should exponentially increase with increasingly negative voltage. The experimentally observed current was in between those two limiting cases (Fig. 3 B). A value of 30% was selected because it fitted the experimental I-V relationship best. The experimentally measured anion current was assumed to be directly proportional to the sum ($\overline{N_2TG}$ + $0.3\,\overline{N_2T'G}$), the unitary anion current carried by a single transporter in the state $\overline{N_2TG}$, and the number, *N*, of transporters under observation.

When glutamate binding becomes rate limiting at low glutamate concentrations, the apparent rate of formation of $\overline{N_2TG}$ and, thus, the current rise, $1/\tau_{app}$, can be described as follows:

$$\frac{1}{\tau_{app}} = k_{+1,app}[Glu] + k_{-1,app}. \quad (1)$$

The rate constants for binding, k_{+1}, and dissociation, k_{-1}, are apparent rate constants in this equation, since they are determined also by preceding and subsequent ion binding equilibria, respectively (see Scheme 1):

$$k_{+1,app} = k_{+1}\frac{[Na^+]}{[Na^+] + K_{Na+1}} \quad (2)$$

$$k_{-1,app} = k_{-1}\frac{K_{Na+2}}{[Na^+] + K_{Na+2}}. \quad (3)$$

Here, K_{Na+1} and K_{Na+2} represent the dissociation constants of Na^+ from its binding site on the glutamate-free, and glutamate-loaded transporter, respectively. For simplicity, we have neglected binding of the third sodium ion, since our data do not allow us to differentiate whether it binds before or after glutamate binding. When glutamate binding is rate limiting, the current rise, which is proportional to $[\overline{N_2TG}]$ (see below), can be described by a single exponential function:

$$[\overline{N_2TG}](t) \approx 1 - \exp(-(k_{+1,app}[Glu^-] + k_{+1,app} + k_{ss}) \cdot t) \quad (4)$$

with k_{ss} being the steady-state turnover number at saturating glutamate concentrations.

At higher glutamate concentrations, where binding is in rapid preequilibrium with respect to the other reactions, and under forward transport conditions (glutamate translocation is assumed to be irreversible), the steady-state population of $\overline{N_2TG}$ can be described as

$$[\overline{N_2TG}]_{ss} = \frac{[Glu^-]}{[Glu^-] + K_m}\frac{k_t k_{-2}}{k_t k_{-2} + k_{-2}k_r + k_t k_r} \quad (5)$$

with

$$K_m = K_{d,app}\frac{k_{-2}k_r}{k_t k_{-2} + k_{-2}k_r + k_t k_r} \quad (5A)$$

and

$$K_{d,app} = K_d\frac{K_{Na+1} + [Na^+]}{[Na^+]}\frac{K_{Na+2}}{K_{Na+2} + [Na^+]}. \quad (5B)$$

In this equation, $K_{d,app}$ is an apparent equilibrium constant for glutamate binding that is affected by preceding and subsequent Na^+ binding reactions (defined by the equilibrium dissociation constants K_{Na+1} and K_{Na+2}) (Eqs. 2 and 3), and the intrinsic dissociation constant for glutamate, K_d. Eq. 5 was used to model the dependence of K_m on the extracellular Na^+ concentration and the transmembrane potential. For simplicity, only two of the three Na^+ ions cotransported with glutamate were considered.

The apparent rate constant for the decay of the presteady-state current at high glutamate concentrations can be described as follows, assuming that glutamate binding is in rapid preequilibrium:

$$1/\tau = k_r + k_t\frac{[Glu^-]}{[Glu^-] + K_m}. \quad (6)$$

To model the time dependence of the anion current at saturating glutamate concentrations, we used numerical integration of the rate equations describing Scheme 1, in order to determine the change of concentration of $\overline{N_2TG}$ as a function of time.

The voltage dependence of the current was introduced by (a) the voltage dependence of the rate constants k_t and k_{-2}

$$k_t(V_m) = k_t(0)\exp\left(\frac{-z_Q F V_m}{2RT}\right) \quad (7)$$

$$k_{-2}(V_m) = k_{-2}(0)\exp\left(\frac{-z_Q F V_m}{2RT}\right) \quad (8)$$

$$k_r(V_m) = k_r(0)\exp\left(\frac{-z_Q F V_m}{2RT}\right) \quad (9)$$

and (b) the voltage dependence of the unitary anion current, which was calculated according to the Goldman-Hodgkin-Katz current (GHK) equation (Goldman, 1943; Hodgkin and Katz, 1949):

$$I_{SCN} = \frac{P_{SCN}F^2V_m}{RT}\frac{([SCN^-]_i - [SCN^-]_o\exp(-V_m F/RT))}{1 - \exp(-V_m F/RT)}. \quad (10)$$

Here, F is the Faraday constant, T the temperature, R the gas constant, and P_{SCN} the single-channel permeability. The turnover rate of the transporter was estimated from simultaneously measuring presteady-state charge movement, Q_{ps}, and steady-state current, I_{ss}, in the same cell according to the following equation:

$$k_{ss} = \frac{I_{ss}}{ez_{ss}N} = \frac{I_{ss}z_{ps}}{Q_{ps}z_{ss}}. \quad (11)$$

According to the stoichiometry of other transporter subtypes, z_{ss} was set to +2. The apparent valence for the presteady-state charge movement, z_{ps}, was obtained from the voltage dependence of the charge movement, as outlined in the next paragraphs.

Assuming that glutamate binding to EAAT4 leads to rapid binding of Na^+ to the transporter, as illustrated in Scheme 1, the charge moved during the rapidly decaying phase of the current can be calculated as

$$Q_{fast}(V,[Na^+]) = \frac{Q_{max}[Na^+]}{[Na^+] + K_{Na+2}(V_m)}. \quad (12)$$

In this equation, Q_{max} is a scaling factor and represents the maximum amount of charge movement, which depends on the number of transporters under observation, the elementary charge, and the apparent valence of this charge, z_Q. When evaluated in a voltage-dependent manner, Eq. 12 resembles a Boltzmann-like relationship. The midpoint potential of the charge movement, V_Q, is $[Na^+]$ dependent and can be given as:

$$V_Q = \frac{RT}{z_Q F}\ln\left(\frac{[Na^+]}{K_{Na+2}(0)}\right), \quad (13)$$

The voltage dependence of the charge movement is introduced by the voltage dependence of $K_{Na+2}(V_m)$, which can be expressed as follows (Läuger, 1987):

$$K_{Na+2}(V_m) = K_{Na+2}(0)\exp\left(\frac{z_Q F V_m}{RT}\right), \quad (14)$$

where $K_{Na+2}(0)$ represents the dissociation constant of Na^+ from EAAT4 at $V_m = 0$ mV.

RESULTS

Expression of EAAT4 and Transport Assay

Functional characterization of the EAAT4 glutamate transporter subtype was performed after transient expression in HEK293 cells. Prior to transfection, the cells were analyzed for endogenous expression of the five known glutamate transporters subtypes (unpublished data). Neither PCR, immunocytochemistry, im-

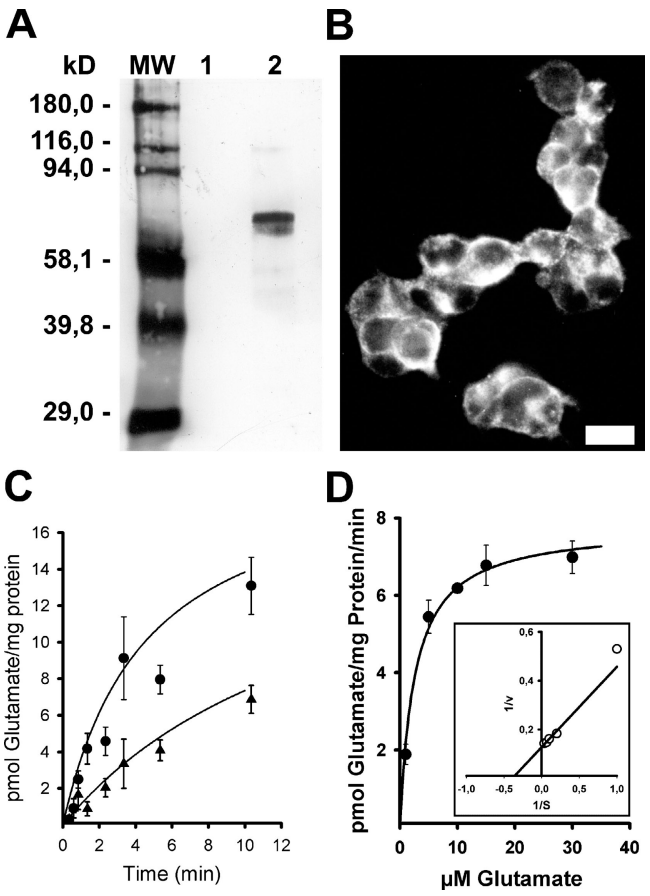

Figure 1. Protein expression and functional characterization of heterologously expressed EAAT4 in HEK293 cells. (A) Immunoblot analysis. Aliquots of SDS extracts (5 μg per lane) of membrane protein fractions of vector alone transfected (lane 1) and HEK_{EAAT4} cells (lane 2) were subjected to SDS-PAGE (10%) and were immunoblotted with EAAC1-specific antibodies (1 μg/ml). Molecular mass markers (lane MW) are indicated in kD. (B) Fluorescence micrograph of HEK_{EAAT4} cells immunolabeled with anti-EAAT4 antibodies (2 μg/ml). EAAT4 immunoreactivity revealed both cytoplasmatic staining and intensely labeled cell boundaries indicating the membranous localization of the heterologously expressed transporter. (Bar, 15 μm). (C) Time course and ionic dependence of glutamate uptake of heterologously expressed EAAT4. The uptake of 1 μCi l-[^{3}H]glutamate was measured for the indicated time periods using membrane vesicle preparations from HEK_{EAAT4} cells at 20 μg protein per time point. The external medium contained 150 mM NaCl (circles) or 150 mM KCl (triangles). Error bars indicate ±SD ($n \geq 4$ sets of triplicate). (D) Kinetic properties of l-[^{3}H]glutamate uptake into HEK_{EAAT4} membrane vesicle preparations. Uptake velocity (in nmol glutamate (min·mg protein)$^{-1}$) was measured by using 1 μCi of l-[^{3}H]glutamate and increasing concentrations of unlabeled l-glutamate at a membrane vesicle protein concentration of 40 μg, and measurements were taken within the linear range of uptake (15 and 30 s). The data presented in the Michaelis-Menten plot are the mean of triplicate determinations from three representative experiments. The K_m and V_{max} values were obtained from the Lineweaver-Burk plot (inset) and represent the mean ± SEM of three independent experiments.

munoblot analysis (Fig. 1 A, lane 1), nor electrophysiological experiments indicated the expression of endogenous EAATs 1–5 in HEK293 cells.

Immunocytochemistry of pCMV-EAAT4–transfected HEK293 cells (HEK_{EAAT4}) with EAAT4-specific antibodies revealed the membranous localization of the heterologously expressed transporter (Fig. 1 B), while non or vector alone–transfected HEK293 cells (mock transfected) showed no staining, neither by immunocytochemistry nor by immunoblot analysis (Fig. 1 A, lane 1). As shown in Fig. 1 A (lane 2), immunoblot analysis demonstrated heterologous expression of the EAAT4 transporter protein with a similar electrophoretic mobility (centered at 65 kD) as determined for the native EAAT4 from rat brain (Furuta et al., 1997; Dehnes et al., 1998).

HEK_{EAAT4} cells mediated Na^+-dependent uptake of glutamate, whereas replacement of external sodium ions by potassium ions inhibited glutamate uptake by >50% (Fig. 1 C). The l-[^{3}H]glutamate uptake as a function of the glutamate concentration demonstrated first order kinetics with a K_m of 2.5 ± 0.7 μM (Fig. 1 D), which is in the same range as determined for the glutamate uptake of EAAT4 expressed in the *Xenopus* oocytes system (Fairman et al., 1995). The V_{max} value (Fig. 1 D; 7.8 ± 1.3 pmol glutamate/min × mg protein) was dependent on the transfection efficiency and varied as much as 10-fold between experiments, whereas the K_m was not affected by varying expression levels. Comparing the K_m values and V_{max} values of EAAT4 with those of EAATs 1–3 in the HEK293 expression system revealed a roughly 100 times lower V_{max} for EAAT4 and an approximately two times lower K_m than that determined for EAATs 1–3. We also determined the V_{max} of EAAT4 for glutamate transport in the presence of SCN^- on both sides of the membrane. This V_{max} was approximately three times larger than the one determined in the presence of only Cl^- (both at saturating glutamate concentrations of 50 μM, $n = 3$), indicating that inclusion of the chaotropic anion SCN^- in the solutions does not inhibit EAAT4, but may lead to a slight stimulation of uptake. Although there was a 1.5-fold [SCN^-] gradient across the membrane that could affect the membrane potential (in the range of −10 mV, the cells were not voltage controlled during uptake) and, therefore, increase the transport rate, this effect cannot fully account for the factor of three determined here. In contrast to the V_{max}, the K_m for glutamate was not affected by the presence of SCN^-.

Properties of EAAT4 Steady-state Currents

We next aimed at determining the kinetic properties of EAAT4 at steady state. Whole-cell recordings of EAAT4-expressing cells after rapid perfusion with glutamate showed a time-dependent inward current, which

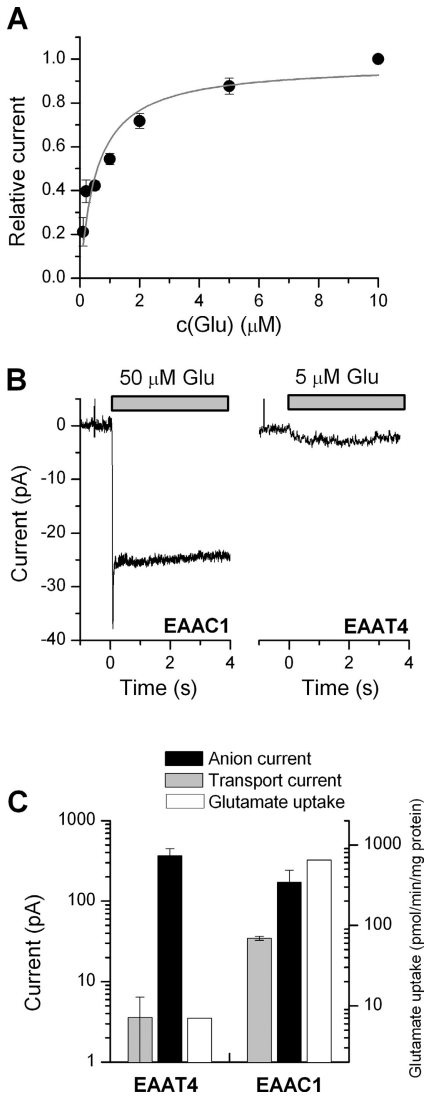

Figure 2. Steady-state transport properties of EAAT4 in comparison to EAAC1. (A) Glutamate concentration dependence of EAAT4 whole-cell currents. The extracellular [Na^+] was 140 mM at pH 7.4. Currents were normalized to the current obtained at 10 μM glutamate. Data were fitted to the Hill equation with a K_m value of 0.6 ± 0.12 μM (line). (B) Typical transport currents recorded from HEK293 cells expressing EAAC1 (left) and EAAT4 (right) induced by extracellular application of 50 and 5 μM glutamate (indicated by the bar), respectively. The membrane potential was 0 mV. (C) Statistical analysis of transport and anion currents (left axis) and the rate of glutamate uptake (right axis) of HEK293 cells expressing EAAC1 and EAAT4. The difference in steady-state glutamate transport rates and currents between EAAT4 and EAAC1 were not caused by different protein expression levels. According to presteady-state analysis (Eq. 11), the average numbers of transporters in the HEK cell membrane were (2.0 ± 1.5) × 10^6 for EAAT4 and (3.0 ± 0.2) × 10^6 for EAAC1. Anion currents were measured in the presence of intracellular SCN^-.

reached a steady-state level in ~80 ms. This current was dependent on the glutamate concentration. The apparent dissociation constant for glutamate, K_m, at 140 mM Na^+ was determined as 0.6 ± 0.1 μM (n = 7) at 0 mV (Fig. 2 A). This result shows that EAAT4 transports glutamate with high affinity, in line with previous results obtained in the *Xenopus* oocyte expression system (Fairman et al., 1995; Lin et al., 1998).

Steady-state EAAT4 transporter currents were composed of three different components: a glutamate-dependent Na^+/K^+-coupled transport current, a glutamate-induced anion current, and a glutamate-independent current, which we will further refer to as the anion leak current. Each of these currents will be analyzed separately.

Na^+/K^+-coupled Transport Currents

These currents were investigated with only the impermeable anion methanesulfonate (MeS) present in the pipette and bath solution. Under these conditions, we expected to measure the coupled transport current catalyzed by EAAT4 in isolation. Application of 50 μM glutamate to the cells induced only small coupled transport currents in HEK_{EAAT4} (Fig. 2 B, right). Currents were only observed in cells with high expression levels of EAAT4. We observed currents only in ~10% of the transfected cells. This current was inwardly directed with an average amplitude of 3.6 pA ± 2.8 pA (n = 12 cells, Fig. 2 C). In contrast, an average transport current of 34.6 ± 2.0 pA was observed in HEK293 cells expressing EAAC1 (Fig. 2 B, left; average value shown in Fig. 2 C). These results are in line with the higher rate of glutamate uptake in EAAC1-expressing cells compared with EAAT4 (Fig. 2 C), supporting the assumption that the transport cycle is significantly faster in the EAAC1 subtype than in EAAT4. It should be noted that we expected even smaller transport currents from the results of the glutamate uptake studies. However, it is not possible to quantitatively compare transport currents with glutamate uptake rates into membrane vesicles because we cannot determine the relative contribution of EAAT4 protein to the total amount of protein in the membrane vesicle preparation. Steady-state transport currents (7.5 ± 12 pA, n = 3) were also observed when SCN^- was present at equal concentrations (140 mM, 0 mV transmembrane potential) on both sides of the membrane. The reversal potential of the glutamate-induced current was shifted to + 2 mV, compared with the 0 mV expected for pure anion current. Thus, these results confirm the data from the uptake experiments, showing that electrogenic glutamate transport is not inhibited by the presence of SCN^-.

Glutamate-dependent Anion Current

We used the highly permeant SCN^- ion to substitute Cl^- in the intracellular solution, resulting in a dramatic increase of the anion current, as already described for other transporter subtypes (Bergles et al., 2002). Under these conditions, application of 100 μM glutamate to

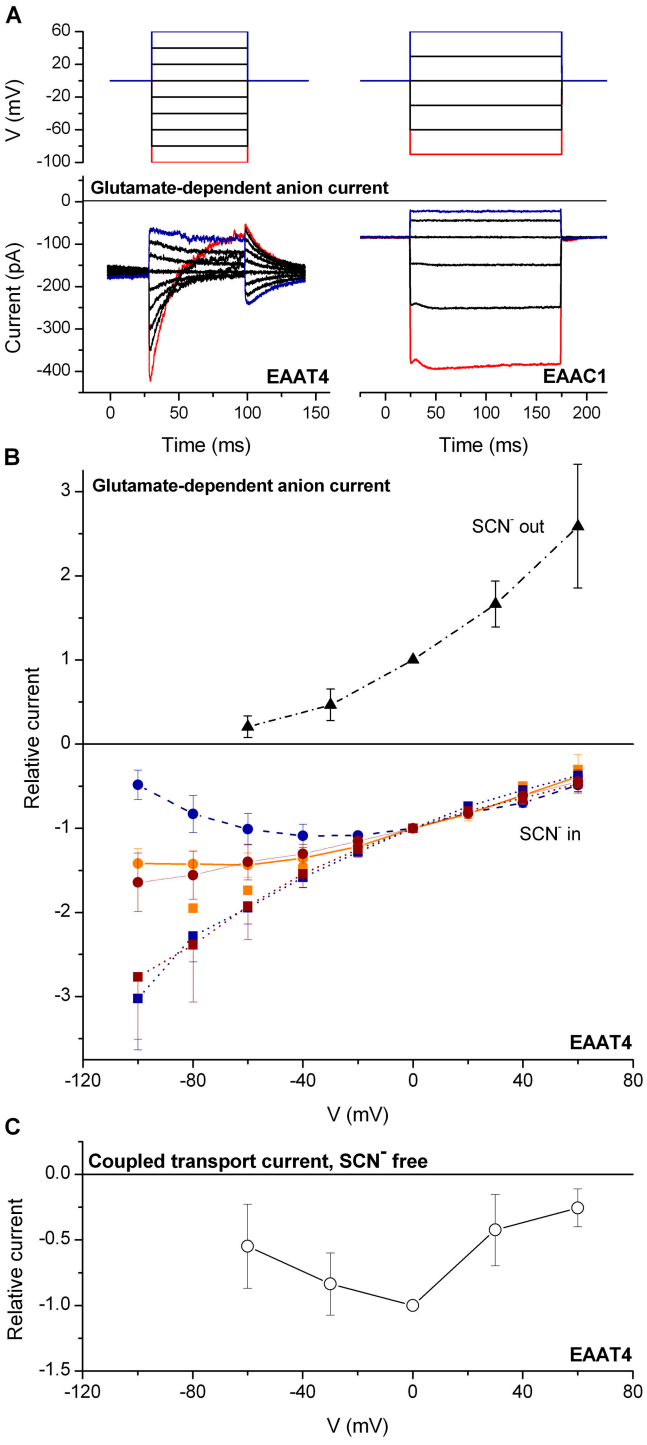

Figure 3. Voltage jump–induced current relaxations in EAAT4 and EAAC1. (A) Top trace, voltage jump protocol used to measure glutamate-dependent currents shown in the bottom trace, the protocol starts at −100 mV and ends at 60 mV (EAAT4, left), and −90 to 60 mV (EAAC1, right); bottom trace, a typical signal obtained through subtraction of current traces recorded with glutamate from the control traces without glutamate for EAAT4 (left) and EAAC1 (right). Data were recorded at forward transport conditions (140 mM KSCN intracellular). (B) Voltage dependence of maximum currents relative to the current at 0 mV in the presence of 140 mM SCN^- outside the membrane (black, closed triangles) determined with a voltage ramp protocol. Traces below the 0 line were performed with SCN^- substituting Cl^- in the pipette solution. All of these traces were recorded with a voltage jump protocol shown in A. Blue traces indicate measurements with 140 mM potassium in the pipette, transient (squares) and steady-state currents (circles) were plotted separately. Orange traces were recorded under homoexchange conditions with 140 mM sodium and 10 mM glutamate inside the cell; circles correspond to transient currents, squares to steady-state current, respectively. Magenta traces represent currents measured with oocyte ringer and internal solution similar to conditions inside oocytes (see main text). (C) Steady-state current–voltage relationship of the coupled transport current recorded in the absence of permeant ions (MeS susbtitution) with a voltage ramp protocol. The glutamate concentration was 100 μM.

EAAT4 resulted in an average anion current of −370 ± 80 pA (Fig. 2 C, $n = 12$). This current was ∼100 times larger than the coupled transport current, demonstrating that anion flux can be studied in isolation. This result is in agreement with previous reports, showing that EAAT4 currents generated by glutamate in *Xenopus* oocytes are mainly carried by anions (Fairman et al., 1995; Mitrovic et al., 2001). In previous investigations, l-aspartate was used as a transported substrate for EAAT4 instead of l-glutamate (e.g., Eliasof et al., 2001). Therefore, we compared the maximum anion current activated by 100 μM aspartate with that evoked by 100 μM glutamate. We obtained an aspartate/glutamate current ratio of 1.5 ± 0.4 ($n = 4$), confirming a previous report that aspartate generates a larger anion current in EAAT4 than glutamate (Fairman et al., 1995).

To test whether the glutamate-induced current in the presence of SCN^- was carried by anions, experiments were performed at different transmembrane potentials and after reversing the anion gradient across the membrane (Fig. 3). First, SCN^- was applied only to the extracellular side of the membrane while the transporter was activated by 100 μM glutamate in the forward transport mode (Fig. 3 B, SCN^- out, black triangles). Under these conditions, currents were outwardly directed and increased with increasing membrane potential. This behavior is in line with previous findings for EAAC1 (Watzke et al., 2001) and EAAT2 (Melzer et al., 2003) and is due to the increase in the driving force for SCN^- inflow at increasingly positive voltages, according to the GHK equation (Goldman, 1943; Hodgkin and Katz, 1949).

When SCN^- was only present at the intracellular side, the current–voltage relationship at steady state showed a different, unexpected behavior (Fig. 3 B, blue circles). Whereas the inward current induced by 100 μM glutamate increased with increasingly negative voltages at potentials up to −20 mV, it reached a maximum at −20 to −40 mV and declined at more negative transmembrane potentials. This indicated that the gluta-

mate-induced EAAT4 anion current was inhibited by negative voltages. To further test this unusual steady-state current–voltage behavior, we performed voltage jump experiments in the presence of 100 μM extracellular glutamate under forward transport conditions (Fig. 3 A, left). The membrane potential was jumped from a holding potential of 0 mV to values ranging from −100 to +60 mV. Interestingly, the current recorded immediately after the voltage jump followed GHK behavior (Fig. 3 B, blue squares), but the initial transient current relaxed to a new steady-state value with an almost voltage-independent time constant in the range of 15 ms ($\tau = 14 \pm 3$ ms, $n = 3$). As expected from the steady-state experiments, the final level of the current recorded at 75 ms after the voltage jump showed a bell-shaped current voltage relationship, showing time-dependent inhibition of the anion current after jumps to very negative potentials, and a slight activation of the current after jumps to positive potentials. Immediately after the end of the square-wave voltage pulse, when the voltage was jumped back to 0 mV, activation of EAAT4 anion current at positive voltages (+60 mV) was still observed since the current increased beyond its initial value at 0 mV before the voltage pulse (I/I(initial) = 1.4 ± 0.1, $n = 3$). On a much slower time scale the current relaxed back to its initial value with a time constant of 16 ± 4 ms ($n = 3$). These results show that the conversion between the inhibited and activated anion-conducting states is a relatively slow process, while the change in the driving force for the anion leads to a fast, submillisecond change in the anion current.

One possible explanation for the inhibition of the anion current at negative transmembrane potentials would be that rapid anion efflux leads to a SCN^- depletion of the intracellular solution. However, this possibility is unlikely for three reasons. (1) Voltage jumps applied to cells expressing EAAC1 did not show any time-dependent relaxation behavior, even in cells that had the same or higher absolute anion current (Fig. 3 A). (2) We did not observe any difference in the relaxation behavior of the EAAT4 anion current when recording from cells of different sizes and transporter expression levels, as would be expected if intracellular anion depletion would occur. (3) We estimated that, based on an average current of 500 pA at −90 mV and a cell diameter of 20 μm, cytosolic SCN^- would be depleted maximally by 5% within 75 ms (the time of the voltage jump), even in the total absence of SCN^- inflow from the pipette to the cytosol.

A second possible explanation of these results is that upon jumping the voltage to negative values EAAT4 accumulates in a state with low anion conductance within the transport cycle. Since it was shown before that for other transporter subtypes the K^+-induced relocation step is most likely rate limiting, it can be speculated that this low-conductance state is associated with the K^+-dependent branch of the transport cycle. To test this possibility, EAAT4 anion currents were investigated in the homoexchange mode in the absence of K^+ and the presence of intracellular Na^+ and glutamate. In the homoexchange mode, the whole transport cycle cannot be completed (Scheme 1, gray area). After voltage jumps from 0 to −90 mV, currents showed a transient component and a relaxation to a new steady state, although not as pronounced as in the forward transport mode (Fig. 3 B). The current–voltage relationship of the steady-state component was almost linear, although the current slightly levelled off at negative voltages, but did not decrease (Fig. 3 B, orange circles). The transient component followed the expected GHK behavior (Fig. 3 B, orange squares). These data indicated that inhibition of the steady-state anion current is less pronounced in the homoexchange mode than in the forward transport mode.

Finally, we asked the question of why the unusual current–voltage relationship of EAAT4 has not been observed so far in previous reports based on electrophysiological data (Fairman et al., 1995, 1998; Mitrovic et al., 2001; Melzer et al., 2003). In most of these reports, EAAT4 was studied in *Xenopus* oocytes. To answer this question, the experiments were repeated under ionic conditions that equal those typically used in oocyte recordings (external oocyte Ringer solution and a pipette solution that mimics the ion composition in oocytes of 10 mM Na^+ [Deitmer et al., 2003] and 5 mM glutamate; 5 mM is a conservative estimate, the real value is probably closer to 10 mM [Seal et al., 2001]). The steady-state currents (magenta circles) show a similar time course as those found in the homoexchange mode. The steady-state current–voltage relationship is almost linear, which is in agreement with the previous reports using the oocyte expression system. Therefore, it is reasonable to assume that EAAT4 currents measured in oocytes kinetically resemble the exchange mode of EAAT4.

When SCN^- was neither present in the pipette nor in the bath solution (replaced by MeS) a current–voltage relationship was observed, which is different from the transporter subtypes EAATs 1–3 expressed in the same cell line (Grewer et al., 2000; Otis and Kavanaugh, 2000; Bergles et al., 2002). Under these ionic conditions, the transport component of the current is measured. Starting at −60 mV the current increased to a maximum at 0 mV while a further increase of voltage leads to a decreasing current (Fig. 3 C). Therefore, inhibition of transporter function at negative potentials is not limited to the EAAT4 anion conductance, but also observed for electrogenic glutamate transport, suggesting that the turnover number of EAAT4 decreases at negative membrane potentials.

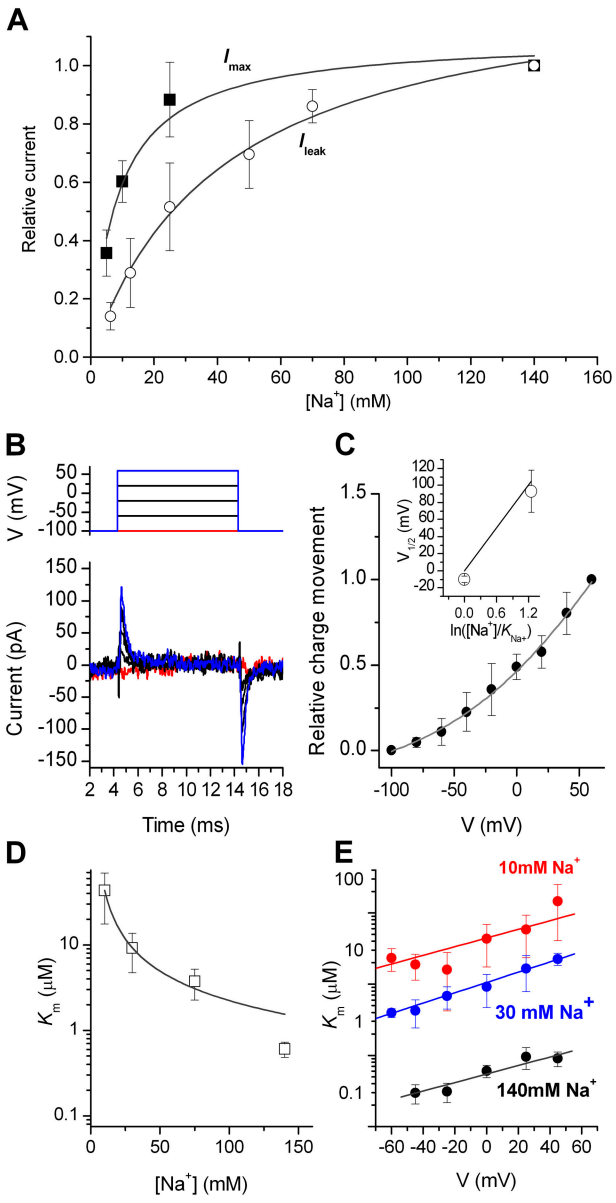

Figure 4. Binding of Na^+ to the empty transporter and the glutamate-bound form. (A) Sodium concentration dependence of the maximum whole-cell current (I_{max}, closed squares) at saturating glutamate concentrations (currents at 5 mM [1 mM Glu], 10 mM [1 mM Glu], and 20 mM Na^+ [0.5 mM Glu] were normalized relative to the current at 140 mM Na^+ [0.1 mM Glu]). The solid line represents a fit with the Hill equation with a K_m= 8.4 ± 1.9 mM. The open circles show the [Na^+] dependence of the glutamate-independent leak current (I_{leak}). The Hill equation was used to fit the data. The apparent K_m is 42.3 ± 5.2 mM. (B) Typical current relaxations in the empty transporter after voltage jumps from a holding potential of −100 mV to the potential specified in the voltage jump protocol shown in the top panel. The extracellular Na^+ concentration was 140 mM. Currents were corrected for unspecific leak components by subtraction of a trace obtained under the same conditions, but in the presence of 100 μM TBOA. The anion in the extracellular and intracellular solutions was MeS. (C) Voltage dependence of the charge movement, obtained by integrating the transient currents shown in B. The charge movement was normalized to that obtained at +60 mV. The solid line represents a fit to the Boltzmann equation with a midpoint potential of 95 mV and a z_Q of 0.3. The inset shows the dependence of the midpoint potential on [Na^+]. The solid line shows the expected dependence based on the kinetic parameters listed in Table I. (D) Sodium concentration dependence of the apparent K_m for glutamate. The solid curve represents a fit obtained by application of Eq. 5B (MATERIALS AND METHODS). Parameters used were K_{Na+1} = 46 mM and K_{Na+2} = 9 mM. (E) [Na^+] and voltage dependence of the apparent K_m of EAAT4 for glutamate. The black trace represents the influence of voltage on K_m at 140 mM Na^+. The blue (30 mM Na^+) and red (10 mM Na^+) traces have been recorded with NMG^+ as a substitute for sodium ions. The lines represent linear fits on the semi-log scale. The slope does not differ significantly at the different conditions: (6.0 ± 1.9) × 10^{-3} /mV, 140 mM Na^+, (7.2 ± 1.1) × 10^{-3}/mV, 30 mM Na^+, and (6.1 ± 3.7) × 10^{-3}/mV, 10 mM Na^+.

Na^+ Binding to the Empty Transporter

In EAAC1 and other transporters of the same family a leak anion current was observed, which is independent of the presence of glutamate (for review see Grewer and Rauen, 2005). In EAAT4, this leak anion current is also present, in agreement with a previous report by Melzer et al. (2003). The leak current was induced by application of Na^+ to the transporter (unpublished data), suggesting that Na^+ binding in the absence of glutamate is required for leak anion current activation. In the presence of 140 mM intracellular SCN^-, the leak current had an average amplitude of 73 ± 18 pA (n = 2). In contrast, nontransfected cells responded to 140 mM Na^+ application with a much smaller current of 9 ± 0.5 pA. To test the apparent affinity of the Na^+ binding site on the empty transporter, we measured the leak anion current in dependence of the sodium concentration in the extracellular solution (Fig. 4 A). The current was fitted by means of a Michaelis-Menten–like equation, obtaining an apparent K_m of 42 ± 5 mM.

Next, we tested whether Na^+ binding to the glutamate-free form of EAAT4 is electrogenic. As shown in Fig. 4 B, step changes in the membrane potential form a holding potential of −100 mV to more positive potentials of up to +60 mV elicited transient, outwardly directed currents that decayed with a time constant in the 0.5 ms range (140 mM [Na^+]). When the voltage was stepped back to −100 mV a transient current in the opposite direction was observed. To test whether these transient currents are associated with Na^+ binding, as has been proposed for other EAAT subtypes, we determined the voltage and [Na^+] dependence of the voltage jump–induced charge movement. As shown in Fig. 4 C, the charge movement started to level off at very negative voltages, an indication that voltage drives the transporter into the fully Na^+-bound state under these conditions. The midpoint potential of the charge movement was estimated as +93 ± 25 mV (Fig. 4 C, inset). This observation is in agreement with

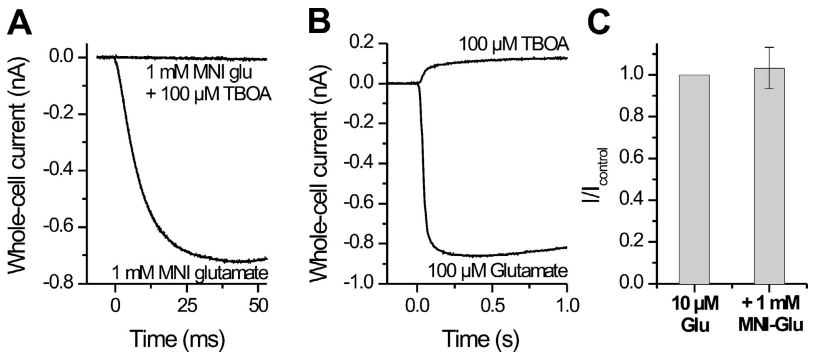

Figure 5. Photolysis of MNI-glutamate can be used to rapidly activate currents in EAAT4. (A) Photolysis of 1 mM MNI glutamate results in activation of inwardly directed anion current, which is inhibited by the coapplication of 100 µM TBOA (top trace). (B) Control experiments of anion currents elicited by EAAT4 (140 mM KSCN in the cytosol). The application of 100 µM TBOA blocks a leak anion current, showing that TBOA binds to the transporter. (C) 1 mM MNI glutamate does not inhibit anion currents activated by 10 µM glutamate. All experiments were performed at 0 mV transmembrane potential.

the K_m for Na^+ binding of 42 mM determined above, which suggests that at an extracellular [Na^+] of 140 mM the transporter is predominantly present in the sodium-bound form. When the extracellular [Na^+] was lowered to 40 mM, a value close to the K_m, the midpoint potential of the charge movement shifted to -10 ± 4 mV (Fig. 4 C, inset), indicating that more negative voltage was necessary to drive Na^+ into its binding site on EAAT4. These results suggest that Na^+ binding to its extracellular binding site, or a conformational change associated with it, generates the transient charge movement induced by the voltage jumps. The apparent valence of this charge movement was estimated as 0.3.

Sodium Concentration Dependence of EAAT4 Steady-state Kinetics

The value of the maximum glutamate-induced anion current is [Na^+] dependent at steady state and is saturated at physiological Na^+ concentrations (Fig. 4 A). The currents shown in Fig. 4 A were obtained at saturating concentrations of glutamate (see legend to Fig. 4 for the concentrations used) at the respective Na^+ concentration (I_{max}) and were normalized to the maximum current at 140 mM Na^+. At 0 mV the apparent K_m for Na^+ was determined as 8.4 ± 1.9 mM ($n = 3$), which is significantly lower than the apparent K_m determined for EAAC1 ($K_m = 22$ mM) under the same conditions (Watzke et al., 2001). These results demonstrate that high glutamate concentrations cannot compensate for low Na^+ concentrations in the extracellular solution, suggesting that at least one Na^+ ion binds to EAAT4 after glutamate is bound. Furthermore, we determined the effect of [Na^+] on the apparent K_m for glutamate. As shown in Fig. 4 D, the K_m increases with decreasing [Na^+]. This result is in line with previous studies on EAAC1 showing that the presence of sodium ions is necessary for high-affinity glutamate binding (Kanai et al., 1995; Watzke et al., 2001).

In other glutamate transporter subtypes, the K_m values for glutamate and competitive inhibitors are not strongly dependent on the transmembrane potential, leading to the suggestion that glutamate binding is electroneutral (Wadiche et al., 1995b; Grewer et al., 2000). To test this idea, we determined the voltage dependence for K_m of EAAT4. At a sodium ion concentration of 140 mM the K_m for glutamate is weakly voltage dependent (slope of the log[K_m] vs. V plot was $[6.0 \pm 1.9] \times 10^{-3}$/mV), decreasing at more negative transmembrane potentials (Fig. 4 E, black circles). When the same experiment was repeated at decreasing sodium concentrations (30 mM, blue circles, and 10 mM, red circles), The K_m was shifted to higher values, as shown above, but the steepness of the K_m–voltage curve remained almost the same ($[7.2 \pm 1.1] \times 10^{-3}$/mV, 30 mM Na^+, $[6.1 \pm 3.7] \times 10^{-3}$/mV, 10 mM Na^+). These results are not consistent with electrogenic glutamate binding, since the opposite voltage dependence of K_m would be expected in this case. However, the results can be explained by a simple model shown in Scheme 1, as will be described in the DISCUSSION section.

TABLE I

Kinetic Parameters and their Respective Apparent Valences, z_Q, Used for the Simulations Shown in Fig. 10

	$k_{+1/-1}$	$k_{+t/-t}$	k_{-2}	k_r	k_{ss}	K_{Na+1}	K_{Na+2}
	$(M^{-1}s^{-1})/(s^{-1})$	(s^{-1})	(s^{-1})	(s^{-1})	(s^{-1})	(mM)	(mM)
	$2 \times 10^7/50$	14/14	200	20	7.9	50	8.4
z_Q	0	+0.7	+1.5	−1.0	+2.0	+0.3	+0.5

Presteady-state Kinetics of EAAT4 Currents

We used the technique of laser-pulse photolysis of caged glutamate in order to generate glutamate concentration jumps on the submillisecond time scale. Photolysis of 1 mM MNI-glutamate resulted in the generation of large, inwardly directed anion currents in the presence of intracellular SCN^- (Fig. 5 A). These currents were specifically carried by the recombinantly expressed EAAT4, since the presence of 100 µM TBOA (dl-*threo*-β-benzyloxyaspartate), a competitive inhibitor of glutamate transport, completely inhibited the activation of the inward current upon photolysis (Fig. 5 A). As expected (Shigeri et al., 2001), TBOA was an inhibitor of EAAT4, since application of TBOA to the cells in the absence of glutamate resulted in inhibition of the leak anion conductance (Fig. 5 B), a typical property of

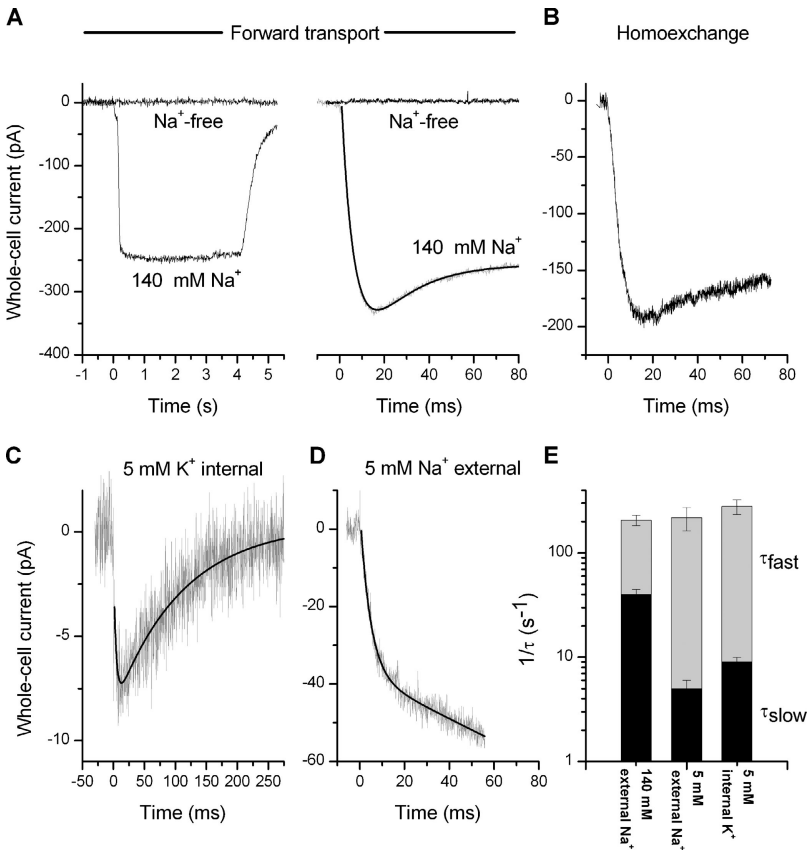

Figure 6. Presteady-state properties of the anion currents catalyzed by EAAT4. (A) Typical whole-cell currents recorded from HEK_{EAAT4} cells induced after rapid application of glutamate at time $t = 0$ by rapid solution exchange (50 μM, left) or photolysis of 500 μM MNI-caged glutamate (30 ± 5 μM released, right) to the same cell in the absence (top traces) and presence (bottom traces) of 140 mM extracellular Na^+ (V = 0 mV, 140 mM KSCN-based intracellular solution). (B–D) Currents induced by photolytic release of glutamate from MNI-glutamate as described in A, but in the homoexchange mode (B, NaSCN-based intracellular solution with 10 mM internal glutamate), in the presence of only 5 mM intracellular K^+ (C), and in the presence of only 5 mM extracellular Na^+ (D). (E) Comparison of the relaxation rates $1/\tau_{fast}$ (gray bars) and $1/\tau_{slow}$ (black bars) of the anion current at different concentrations of extracellular Na^+ and intracellular K^+. The membrane potential was 0 mV.

competitive glutamate transporter inhibitors (Campiani et al., 2001). Next, we tested whether MNI-glutamate inhibits EAAT4 activity. As shown in Fig. 5 C, coapplication of 1 mM MNI-glutamate together with 10 μM glutamate did not lead to a reduction of the current compared with the control (10 μM glutamate alone), suggesting that at concentrations up to 1 mM, MNI glutamate does not inhibit the function of EAAT4. The typical concentration of MNI-glutamate used in the following experiments was 500 μM. Finally, application of 1 mM MNI-glutamate to EAAT4-expressing cells did not induce any measurable anion current (unpublished data), suggesting that MNI-glutamate is not a substrate of EAAT4. Together, these results suggest that MNI-glutamate is a suitable caged substrate for presteady-state kinetic studies of EAAT4.

To characterize the presteady-state kinetics of glutamate transport by EAAT4, we first performed experiments in the anion conducting mode (Fig. 6 A). Rapid application of 50 μM glutamate to EAAT4-expressing cells with a rapid perfusion system resulted in the generation of an inwardly directed anion current within ~100 ms (Fig. 6 A, left). The rate of the rise of this current was limited by the speed of solution exchange around the cell (time constant 50–100 ms). In contrast, application of 30 μM glutamate by photolytic release from 500 μM MNI-glutamate resulted in a much more rapid activation of the anion current with a time constant of τ_{rise} = 4.5 ± 0.3 ms (n = 3, Fig. 6 A, right). In addition, a decaying phase was observed in the photolysis experiment that was absent in the rapid perfusion experiment, due to the limited time resolution of the perfusion method used here. The time constant of the decaying phase was τ_{decay} = 25 ± 0.3 ms (n = 3, 30 μM glutamate). Currents induced by both rapid perfusion and photolytic glutamate release were abolished by removing Na^+ from the extracellular solution, as expected for a Na^+-coupled cotransporter (Fig. 6 A, right and left). So far, experiments were performed in the forward transport mode (KSCN-based pipette solution). Next, we tested whether currents can be also generated in the exchange mode (NaSCN, glutamate-based pipette solution). As shown in Fig. 6 B, photolytic application of 30 μM glutamate to an EAAT4-expressing cell generated a rapidly activating current with kinetics similar to those observed in the forward transport mode (τ_{rise} = 4.2 ± 1.3 ms, τ_{decay} = 21 ± 6 ms, n = 3). As in the forward transport mode, glutamate application induced a sustained steady-state anion current in the exchange mode. A similar behavior has been previously reported for EAAT2 and EAAC1 (Otis and Kavanaugh, 2000; Watzke et al., 2001; Bergles et al., 2002).

In further experiments, we tested the dependence of the glutamate-induced presteady-state currents on the

concentration of co- and counter-transported cations (Fig. 6, C and D). When K^+ in the intracellular solution was replaced with the nontransportable cation NMG^+, application of glutamate did not induce any measurable steady-state or transient currents. This result was expected, since the majority of the transporter binding sites for glutamate were most likely exposed to the cytoplasm under these conditions. In the presence of 5 mM intracellular K^+, some of the transporter binding sites are expected to be driven outward to face the extracellular side. In agreement with this expectation, a small transient anion current with a peak amplitude of I_{peak} = 8 ± 4 pA (n = 3) was observed (Fig. 6 C). However, the current decayed to 0 pA within 250 ms without any steady-state anion current being present (n = 3). This result suggests that upon glutamate binding the transporter passes through anion conducting states, while it becomes locked in a state of lower anion conductance when the empty binding sites for Na^+ and glutamate are exposed to the cytoplasm. A different result was obtained when the experiment was repeated in the presence of 140 mM intracellular K^+, but after reducing the extracellular sodium ion concentration to 5 mM (Fig. 6 D). Under these ionic conditions, the steady-state anion current was still present (47 ± 9 pA, n = 4). However, no transient component of the current was observed. Together, these results indicated that the presence of high extracellular [Na^+], but not high intracellular [K^+] is required for the presence of the transient anion current component. The time constants observed under the different ionic conditions are summarized in Fig. 6 E.

Dependence of Presteady-state Kinetics on the Extracellular Glutamate Concentration

To further assign the two phases of the glutamate-induced anion current, we determined the dependence of the anion current on the extracellular glutamate concentration (Fig. 7). Typical current recordings at glutamate concentrations of 0.5, 1.2, and 35 μM are shown in Fig. 7 A. At 0.5 μM glutamate, the current rises slowly to a new steady-state level (τ_{rise} = 48 ± 11 ms, n = 3), but the transient component of the current was not observed anymore. This behavior was reminiscent of that observed at low extracellular [Na^+], a result that supports a previous report on EAAC1 (Watzke et al., 2001) where it was found that changing either extracellular [Na^+] or [glutamate] has similar effects on the time dependence of the anion current. The [glutamate] dependencies of the relaxation rate constants, $1/\tau$, for the rising phase and the decaying phase of the current are shown in Fig. 7 B. Both relaxation rates level off at high glutamate concentration, a behavior that is indicative of a conformational change following glutamate binding (see Eq. 6). The limiting rates at high glutamate concentrations were 46 ± 11 s^{-1} for the decaying phase and 350 ± 20 s^{-1} for the rising phase of the current. Only at low glutamate concentrations (<2 μM), the $1/\tau$–[glutamate] relationship can be described by a linear equation (Eq. 1, dashed line in Fig. 7 B). It is expected that glutamate binding becomes rate limiting for the rise of the anion current at such low substrate concentrations. From the linear regression analysis shown by the dashed line and according to Eqs. 1 and 2 (MATERIALS AND METHODS), an apparent bimolecular rate constant for glutamate binding to EAAT4 of (1.1 ± 0.4)*10^7 $M^{-1}s^{-1}$ was estimated ($k_{+1,app}$, Eqs. 1, 2, and 3). This value is in good agree-

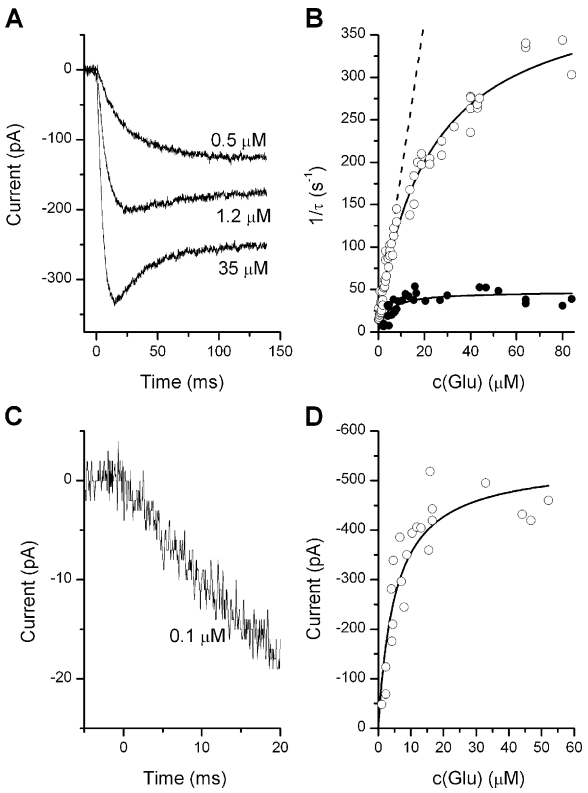

Figure 7. Dependence of EAAT4 presteady-state anion currents on the glutamate concentration. (A) Typical anion currents induced by photolysis of 500 μM MNI-glutamate at different laser energies, releasing 0.5, 1.2, and 35 μM free glutamate. (B) Dependence of the relaxation rate constant $1/\tau$ on the glutamate concentration. The open and solid circles correspond to the relaxation rate constants for the rising phase and the decaying phase, respectively. The solid lines represent fits to Eq. 6 with K_m values and maximum relaxation rates of 12 ± 5 μM and 350 ± 20 s^{-1} (rising phase), and 0.6 ± 0.2 μM and 46 ± 11 s^{-1} (decaying phase), respectively. The dashed line represents a linear fit to the data obtained from the rising phase with a slope of (1.1 ± 0.4)*10^7 $M^{-1}s^{-1}$ and an intercept of 20 ± 2 s^{-1}. (C) Anion current induced by photolytic release of 0.1 μM glutamate shown at high time resolution. Note the absence of a lag phase. (D) Dependence of the presteady-state current amplitude on the glutamate concentration. The line represents a fit to a Michaelis-Menten–like equation with a K_m of 5.1 ± 1.2 μM.

ment with binding rates previously determined for other subtypes (Grewer et al., 2000; Bergles et al., 2002). The intercept of the linear relationship was calculated as 18 ± 2 s^{-1}. It is likely that this value reflects the apparent rate of glutamate dissociation from its EAAT4 binding site ($k_{-1,app}$, Eqs. 1 and 3), suggesting that glutamate has a long residency time on EAAT4, once it is bound. To further test for rate limitation of glutamate binding at low concentrations, we recorded the anion current rise with high time resolution at an extracellular glutamate concentration of 100 nM (Fig. 7 C). If glutamate binding was fast, we would expect to observe a rapid lag phase since glutamate has to bind first to the transporter before the anion conductance is activated (Watzke et al., 2001). In contrast to this expectation, no lag phase was observed, but the rising phase followed single-exponential kinetics consistent with glutamate binding being rate limiting (Eq. 4).

Analysis of the glutamate concentration dependence of the relaxation rate constants allowed us to determine the apparent rate constant, but not the intrinsic rate constant of glutamate dissociation from EAAT4 ($k_{-1,app}$, Eq. 3). To get an estimate for k_{-1}, we determined the glutamate concentration dependence of the peak current amplitude of the presteady-state current component, I_{ps}. As shown in Fig. 7 D, I_{ps} saturates with a K_m of 5.1 ± 1.2 μM. This K_m is ~10-fold higher than the apparent K_m for glutamate determined at steady state. Although this is still an apparent K_m, we can use it to estimate a lower limit of k_{-1} of 55 s^{-1}. Together these data show that glutamate initially binds with relatively low affinity, but gets locked into its binding site by subsequent reactions of the transporter that pull the glutamate binding equilibrium toward the bound form. We have made a similar observation previously for EAAC1 (Watzke et al., 2001).

So far, we have described the kinetic properties of the anion component of the current carried by EAAT4. Since it is not clear how the anion conductance of EAAT4 is kinetically coupled to glutamate transport, we next investigated the electrogenic transport component of the current. Rapid application of ~30 μM glutamate to EAAT4 by photolysis of 500 μM MNI-glutamate was followed by an inwardly directed transient current under forward transport conditions (Fig. 8 A). This current was abolished when the experiment was repeated in the absence of extracellular Na^+ (Fig. 8 A, top). The current consists of four phases: a rising phase with a time constant of ~2 ms (n = 4), a major, rapidly decaying phase with a time constant of 4.2 ± 0.8 ms (n = 4), a minor, slowly decaying phase with a time constant of 32 ± 14 ms (n = 4), and a steady-state phase. These results show that at least two rapid, glutamate-induced electrogenic transporter reactions and one electroneutral reaction precede steady-state

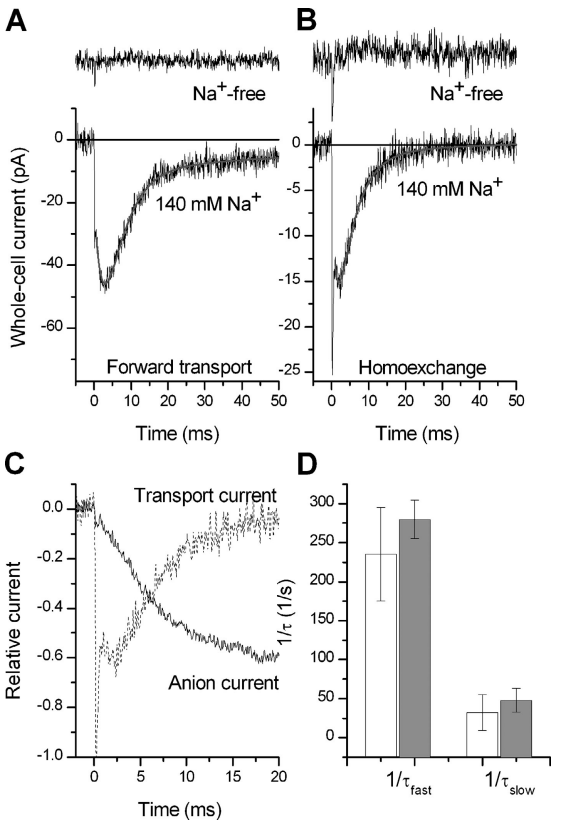

Figure 8. Presteady-state transport currents catalyzed by EAAT4. (A) Transport current induced by photolysis of 500 μM MNI glutamate at time t = 0 in the presence (bottom trace) and absence (top trace) of 140 mM extracellular Na^+. The membrane potential was 0 mV. The pipette contained 140 mM K^+ (forward transport mode). (B) Same experiment as in A, but in the homoexchange mode (140 mM Na^+, 10 mM glutamate in the recording pipette). (C) Comparison of the time courses of the transport current decay and the anion current rise. Both currents were generated by photolysis of 500 μM MNI glutamate. (D) Statistical analysis of the relaxation rate constants of the fast phase and the slow phase of the anion current (gray bars) and the transport current (white bars) at V_m = 0 and [glutamate] = 30 μM. All solutions contained MeS as the main anion.

turnover of EAAT4. To test whether these reactions are associated with the glutamate-dependent branch of the transporter cycle, we repeated the experiments in the exchange mode in the total absence of intracellular K^+, which allowed us to restrict EAAT4 to reactions associated with glutamate translocation (Watzke et al., 2001). Glutamate-induced currents in the exchange mode show the same temporal characteristics of the ones recorded in the forward transport mode (Fig. 8, A and B), except that the steady-state phase is missing. This is expected, since the transporter does not complete a transport cycle in the exchange mode (see Scheme 1). Furthermore, the slowly decaying phase, although present, is somewhat less prominent in the exchange mode (Fig. 8 B).

In EAAC1 the electrogenic transport current precedes the activation of the anion current (Watzke et al., 2001). In Fig. 8 C, the time course of those two current components is compared for EAAT4. The electrogenic transport current decays with a time course that appears to be similar to the time course of activation of the anion current. To quantify this behavior, we have compared the relaxation rate constants for the two phases of the transport and the anion current, as shown in Fig. 8 D. Within experimental error, the relaxation rates for the two components correspond to each other. This result suggests that both current components report the same, glutamate binding–induced molecular rearrangements of the transporter.

Voltage Dependence of Presteady-state Currents

Finally, we determined the dependence of the presteady-state currents on the transmembrane potential. As shown in Fig. 9 A, the relaxation rate constant $1/\tau_{fast}$ increased with increasingly negative transmembrane potential (e-fold/155 mV, see linear fit in Fig. 9 A). In contrast, $1/\tau_{slow}$ was virtually voltage independent (Fig. 9 A, solid circles). The amplitude of the electrogenic glutamate-induced current also depended on the transmembrane potential. The amplitude of the current component associated with τ_{fast} increased with increasingly negative voltage. Fig. 9 B shows the voltage dependence of the charge movement, Q_{fast}, which was obtained by integrating the rapidly decaying component of the electrogenic transport current. At an extracellular [Na^+] of 140 mM, Q_{fast} is only weakly voltage dependent (Fig. 9 B, closed circles). In contrast, Q_{fast} becomes strongly voltage dependent at 10 mM extracellular [Na^+] (Fig. 9 B, open circles). Furthermore, the total charge moved in this process was reduced compared with Q_{fast} obtained at 140 mM Na^+. At 0 mV, the ratio of the charge movements, Q_{fast}(10 mM)/Q_{fast}(140 mM), was 0.28 ± 0.06 (n = 3). We used a Boltzmann relationship (Eqs. 12–14) to fit the experimental data (lines in Fig. 9 B). The data could be represented very well for both extracellular Na^+ concentrations when the apparent valence (z_Q value in the Boltzmann equation) was set to 0.7. The only difference in the two curves is the midpoint potential, $V_{1/2}$, of the charge movement, which was obtained as −30 ± 6 mV at [Na^+] = 10 mM, and +70 ± 9 mV at [Na^+] = 140 mM. These results suggest that the process associated with Q_{fast} is facilitated by both Na^+ and negative voltage, as would be expected for electrogenic Na^+ binding to the glutamate-bound form of the transporter. We were unable to determine the voltage dependence of Q_{slow}, since the associated current amplitude was too small, or the rate of its decay too slow for a quantitative evaluation.

The charge moved during decay of the presteady-state current together with the apparent valence of this charge movement and the steady-state current allowed us to determine steady-state turnover rate, k_{ss}, according to Eq. 11. Since the steady-state current could not be measured in many cells due to the small current amplitude, we can only give an upper limit of the value for k_{ss}. At 0 mV transmembrane potential, this upper limit for the turnover rate was determined as 6 s^{-1}.

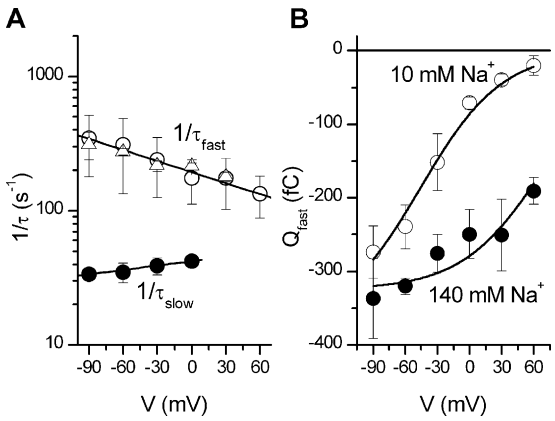

Figure 9. Voltage dependence of EAAT4 presteady-state kinetics. (A) Voltage dependence of the relaxation rate constants for the fast phase (rising phase of the anion current, open circles; rapidly decaying phase of the transport current, triangles) and the slow phase (decaying phase of the anion current, closed circles). (B) Voltage dependence of the charge moved during the fast phase of the transport current at extracellular [Na^+] of 10 mM (open circles) and 140 mM (filled circles). The solid lines represent fits to a Boltzmann Eqs. 12–14.

DISCUSSION

Five glutamate transporter subtypes have been cloned to date. The functional properties of the transporter subtypes 1–3, which have been extensively studied, are very similar to each other, including their kinetics of glutamate transport. Therefore, the question arises: Why do we need so many different subtypes?

Here, we report for the first time that some of the functional characteristics of the subtype EAAT4 are dramatically different from those of the subtypes 1–3, although the transporters share a common transport mechanism. The first new finding of this study is that the glutamate transporter subtype EAAT4 operates 5–10 times more slowly than the transporter subtypes EAATs 1–3 (the kinetic parameters are summarized in Table II). Second, EAAT4 transport has a significantly different dependence on the transmembrane potential than the subtypes 2 and 3. For example, EAAT4 becomes inhibited at very negative voltages and the apparent affinity of EAAT4 for glutamate is dependent on the voltage, whereas that of EAATs 2 and 3 is voltage independent (Wadiche et al., 1995b; Grewer et al., 2000). Third, the affinities of EAAT4 for glutamate and the

TABLE II

Kinetic Parameters of Glutamate Transport by the EAATs 1–4

	EAAT4	EAAC1/EAAT3	EAAT2	EAAT1
K_m (μM)	0.6	8[a]	12[c]	7[f]
K_d (μM)	≥5	50–100[a]	≥140[c]	–
$1/\tau_{fast}$ (s^{-1})	340	1200[b]	4000[c]	1040[f]
$1/\tau_{slow}$ (s^{-1})	34	620[a]	590[c] 930[d]	45[f]
Turnover rate (s^{-1})	<3, extrapolated from −60 mV	90[a]	41[e]	16[f]

All relaxation rate constants and turnover numbers are given for a membrane potential of −80 to −90 mV.

[a]Grewer et al., 2000.

[b]Watzke et al., 2001.

[c]Bergles et al., 2002.

[d]Otis and Kavanaugh, 2000.

[e]Bergles and Jahr, 1998.

[f]Wadiche and Kavanaugh, 1998.

cotransported ion Na^+ are significantly higher than those of EAAC1 (Grewer et al., 2000; Watzke et al., 2001).

Mechanism of Glutamate Transport by EAAT4

The general mechanism of substrate transport by EAAT4 is very similar to those of the previously characterized transporter subtypes. As for EAATs 2 and 3, glutamate transport is based on a sequential mechanism in which glutamate and Na^+ are translocated in the same reaction step, whereas K^+ is counter transported in the relocation reaction of the glutamate-free transporter. Thus, glutamate translocation can still take place in the total absence of intracellular K^+, whereas steady-state turnover is inhibited under these conditions. We assume that the steady-state anion current is mainly rate limited by the K^+-dependent T' to T transition in Scheme 1. The distinct effects of Na^+ and K^+ on glutamate transport by EAAT4 are highlighted by their different effects on the EAAT4 presteady-state current. In the virtual absence of intracellular K^+, glutamate-induced transient anion currents are still present (associated with the glutamate-translocating N_2TG to $N_2T'G$ transition in Scheme 1), but the steady-state anion current component is abolished (Fig. 6 C). In contrast, low extracellular Na^+ concentrations result in inhibition of the transient glutamate-induced anion current component, but steady-state current is still observed (Fig. 6 D). These results indicate that the K^+-induced relocation reaction becomes rate limiting for steady-state turnover at low intracellular [K^+], whereas the Na^+-dependent translocation reaction becomes rate limiting at low extracellular [Na^+].

As in EAAC1, the binding of Na^+ and glutamate to EAAT4 is sequential (Watzke et al., 2001). Glutamate interacts with EAAT4 only after a first Na^+ ion is bound. Thereafter, glutamate binding generates a second, high-affinity binding site for Na^+ on the transporter. The main evidence for this sequential Na^+-glutamate-Na^+ binding mechanism comes from the experimentally determined [Na^+] dependence of the maximum glutamate-induced current at saturating glutamate concentrations (I_{max}), which decreases at low sodium concentrations, showing that at least one Na^+ must bind to the transporter after glutamate is bound. In contrast, if all of the cotransported Na^+ ions would bind to EAAT4 before glutamate, it would be expected that I_{max} is independent of the Na^+ concentration (Watzke et al., 2001). In this case, unless Na^+ binding becomes rate limiting for steady-state transport at very low [Na^+], saturating glutamate concentrations would be expected to pull the Na^+ binding equilibrium toward the bound form, thus overcoming the inhibitory effect of low [Na^+] on the steady-state transport rate. Our results also impose a limit on the stoichiometry of Na^+:glutamate cotransport of EAAT4, which has not been experimentally determined so far. This coupling stoichiometry is at least 2 Na^+:1 glutamate, but is likely to be the same as the 3:1 stoichiometry of EAATs 2 and 3 (Zerangue and Kavanaugh, 1996; Levy et al., 1998).

The rate of steady-state glutamate uptake was somewhat increased in the presence of SCN^- on both sides of the membrane. This effect suggests that SCN^- as a chaotropic anion may have a modulatory role on glutamate transport by EAAT4. Although the rate constants determined from presteady-state kinetic analysis for the glutamate translocation branch of the cycle were the same in the absence and presence of SCN^- (Fig. 8 D), it can be hypothesized that the anion affects the rate of the rate limiting step of the transport cycle in the potassium dependent branch. Additional experiments will be necessary to test this hypothesis. However, these results show that it is important to be cautious about interpreting transport mechanism purely based on data obtained from anion current.

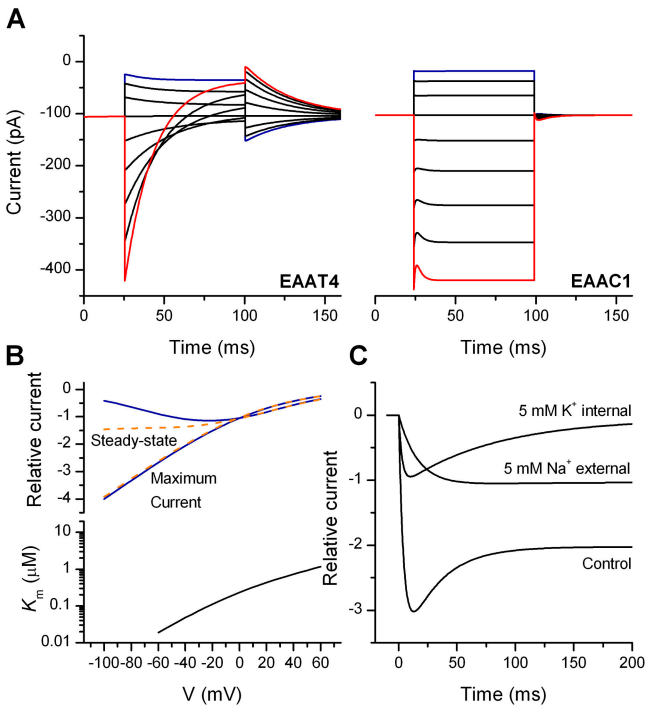

Figure 10. Simulations of steady-state and presteady-state EAAT4 anion currents according to Scheme 1. The parameters used for the EAAT4 simulations are listed in Table I. (A, left) Anion current response of EAAT4 to voltage jumps from a holding potential of 0 mV to values of −100 to + 60 mV in increments of 20 mV (see voltage protocol in Fig. 3 A). The anion current was calculated according to Eq. 10 (140 mM SCN^- in the cytosol) times the population of the anion conducting states as a function of time (obtained from numerically integrating the rate equations pertaining to Scheme 1). The unitary conductance of state $\overline{N_2T'G}$ was set to 30% of that of $\overline{N_2TG}$. (A, right) Anion current response calculated for EAAC1 for the same voltage jump protocol shown in A. The parameters used for EAAC1 were: $k_{+1} = 2 \times 10^7\ M^{-1}s^{-1}$ ($z_Q = 0$), $k_{-1} = 500\ s^{-1}$ ($z_Q = 0$), $k_t = 100\ s^{-1}$ ($z_Q = 0.5$), $k_{-2} = 10000\ s^{-1}$ ($z_Q = 0$), $k_r = 30\ s^{-1}$ ($z_Q = 0.5$). Both Na^+ binding reactions were assumed to be in rapid preequilibrium with an apparent valence of 0.5. (B, top) Simulations of the maximum anion current immediately after the voltage jump and the steady-state anion current for forward transport (blue), and homoexchange (orange) as a function of voltage. (B, bottom) Simulation of the K_m for glutamate as a function of voltage at 140 mM Na^+, according to Eqs. 5A and 5B. (C) Simulation of the time dependence of EAAT4 anion current at 0 mV in the forward transport mode (control, 140 mM Na^+ external), and in the presence of low internal [K^+] and low external [Na^+], according to the experiments shown in Fig. 6.

Voltage Dependence of Glutamate Transport by EAAT4

Interestingly, glutamate transport by EAAT4 has a unique voltage dependence that has not been observed previously. EAAT shows its maximum transport activity close to 0 to −20 mV and inactivates at more negative membrane potentials. This inactivation process takes place with a time constant in the range of 15 ms after a jump of the membrane potential. The inactivation is most prominent under forward transport conditions and is seen to a lesser extent in the exchange mode, suggesting that steps in the potassium-dependent branch of the transport cycle are slow at very negative voltages, thus leading to a trapping of EAAT4 in states that are associated with the potassium relocation. The states associated with the K^+-dependent half-cycle are not anion conducting. Therefore, not only transport, but also the anion conductance is inhibited at negative potentials. In the exchange mode, the states associated with K^+ transport are not accessible, as shown previously for EAAC1 (Watzke et al., 2001). Therefore, inactivation of the anion current is not as prominent in the exchange mode. A simple kinetic model shown in Scheme 1 describes the experimental data very well, as shown in the numerical simulations (Fig. 10, A and B). The model predicts that inactivation at negative potentials is caused by inhibition of either intracellular potassium binding, K^+-induced relocation, or extracellular K^+ dissociation (lumped into transition T' to T in Scheme 1). The apparent valence associated with the respective reaction was calculated as −1, having an opposite sign compared with the apparent valences of any other partial reaction so far observed in glutamate transporters. Thus, this reaction is slowed with increasingly negative transmembrane potentials, whereas the reactions associated with Na^+ binding and glutamate translocation are accelerated. This interpretation is in contrast with previous reports on other glutamate transporter subtypes. In EAAC1, it was proposed that the rate limiting K^+-induced relocation reaction is accelerated at negative potentials because the positive charge moved outward during K^+ transport is overcompensated by negative charges of the cation binding sites (Grewer et al., 2000; Grewer and Rauen, 2005). In agreement with this model, no anion current inactivation is observed at negative potentials (see Fig. 3 A and modeling in Fig. 10 A). The positive charge moved outward during K^+ transport is, therefore, either not compensated by negative charges in EAAT4, or the electrogenic K^+ binding from the intracellular side becomes rate limiting.

A second interesting observation for EAAT4 is that the apparent affinity for glutamate is voltage dependent. The affinity increases with increasingly negative voltages (Fig. 4 E). This behavior is in contrast with EAAC1, which shows a voltage-independent apparent affinity for glutamate, and can be also explained by the simple transport model shown in Scheme 1. According to this model, trapping of glutamate by EAAT4 and regeneration of the free glutamate binding site have the opposite voltage dependence. Therefore, negative voltages lead to more efficient trapping of glutamate and, therefore, higher apparent affinity. This behavior can also be quantified according to Eqs. 5A and 5B, as shown in Fig. 10 B. However, the voltage dependence

of the modeled K_m is slightly steeper than that of the experimentally determined one. The reason may be that there are other partial reactions in the transport mechanism affecting the voltage dependence of EAAT4 transport that were not observed here.

It should be noted that the apparent valences in Scheme 1 were chosen to result in a total of +2 charges being transported in one full cycle. This requires that one H^+ and an additional, third Na^+ ion are cotransported with glutamate, ions that were neglected for simplicity in Scheme 1. Although we have no data on the contribution of the binding and/or transmembrane movement of these two ions to transporter electrogenicity, it is possible that electrogenicity caused by their movement adds to the electrogenicity of some reaction steps shown in Scheme 1. Thus, the valences listed in Table I are apparent values and are not intrinsic to the individual reaction steps shown in Scheme 1, which contain other ion binding reactions not shown.

Comparison with Previous Studies Involving Natively Expressed EAAT4 in Cerebellar Neurons

In two previous reports the presteady-state kinetics of transporters expressed natively in cerebellar Purkinje cells were studied (Otis and Jahr, 1998; Auger and Attwell, 2000). In the first report, the kinetics of the anion conductance of the expressed glutamate transporter were investigated (Otis and Jahr, 1998). These kinetics differ significantly from those of the recombinant EAAT4 reported here. First, the rate of the rise and decay of the transient current component are substantially larger than the rates reported here. For example, the transient component of the glutamate-induced anion current decayed in the Purkinje cell transporter within <50 ms, whereas the transient current of recombinant EAAT4 decays within 100 ms (Fig. 7 B). Second, the ratio of transient to steady-state current is significantly larger in the Otis and Jahr report (Otis and Jahr, 1998) compared with our results. Third, the Purkinje cell transporter has an apparent glutamate affinity in the range of 3 μM, whereas we find values in the submicromolar range. In contrast, the kinetics of the transporter investigated in (Otis and Jahr, 1998) appear to be very similar to those reported by us previously for recombinantly expressed EAAC1 (Grewer et al., 2000), which is also expressed in cerebellar Purkinje neurons (Rothstein et al., 1994; Furuta et al., 1997). In the second report, kinetics of the glutamate-gated anion current, as well as of the transport current, were studied (Auger and Attwell, 2000). Although a direct comparison of the results reported by Auger et al. to our results is more difficult, because the authors applied glutamate to the transporter only for a short period of time (1 ms), it appears that both components of the current show faster kinetics than the EAAT4 current kinetics reported here. Again, these kinetics are more reminiscent of heterologously expressed EAAC1 (Grewer et al., 2000; Watzke et al., 2001). It should be noted that there are two other possible explanations for the different kinetics of recombinant EAAT4 and the native transporters. (1) The natively expressed proteins might be differentially posttranslationally modified in the neurons compared with that of the HEK293 cell system used here. (2) The glutamate concentrations used in the above studies were significantly higher (2 mM) than the maximum of ~100 μM used here. However, since EAAT4 showed saturating behavior at concentrations >50 μM, it is unlikely that the use of higher [glutamate] would result in substantially faster kinetics.

Physiological Significance

EAAT4 is expressed in high levels in the cerebellum, specifically in Purkinje cells (Furuta et al., 1997). Expression in the Purkinje neurons is directed to regions on dendritic spines, which are slightly removed from the excitatory synaptic contacts (Dehnes et al., 1998) where glutamate is released. It is, therefore, likely that presynaptically released glutamate first comes into contact with the low-affinity, high-capacity transporter EAAT2, which is expressed in glia cells that tightly surround the climbing fiber synapses (Bergles et al., 1997). This low-affinity system removes the bulk of released glutamate, but it does not operate effectively once glutamate concentrations reach the low micromolar level. We speculate that the glutamate molecules that escape uptake by glial transporters and diffuse further away from synaptic contacts are removed by the neuronal high-affinity, low-capacity transporter EAAT4. Thus, the main function of EAAT4 might be to prevent spillover to adjacent synapses and to keep the extracellular glutamate concentration at a submicromolar level. However, due to its slow kinetics and its localization removed from the synapse, it is unlikely to be directly involved in terminating the synaptic transmission process, especially because of EAAT4's very low glutamate uptake capacity.

Since EAAT4 is expected to operate at low micromolar to submicromolar glutamate concentrations, it can be speculated that the transporter is not optimized for fast operation. At 0.5 μM concentration, EAAT4 binds only one glutamate molecule every 100 ms. Therefore, capture of glutamate by the transporter is most likely the rate limiting step and other transporter reactions, such as glutamate translocation, are comparatively fast. In contrast, EAAT4 appears to be optimized for tight binding of glutamate. Several factors contribute to this optimization in comparison to the other transporter subtypes: (a) higher affinity Na^+ binding sites result in higher apparent affinity for glutamate; (b) slower dis-

sociation of glutamate leads to tighter binding; (c) the unique voltage dependence of transport results in higher apparent affinity at physiological transmembrane potentials and, thus, to more efficient trapping of glutamate. It will be interesting to determine the molecular basis for this high-affinity optimization of EAAT4.

More efficient trapping of glutamate by EAAT4 at physiological transmembrane potentials is expected to prolong the anion conducting state of this glutamate transporter subtype. The hyperpolarizing action of EAAT4 could counteract the depolarizing action of "low affinity and high capacity" glutamate transporters, such as EAAT3. EAAT3 and EAAT4 are coexpressed in Purkinje cell dendrites (Conti et al., 1998; Dehnes et al., 1998; Kugler and Schmitt, 1999), suggesting a possible cooperative interaction between both transporter subtypes.

This work was supported by National Institutes of Health grant R01-NS049335-02 awarded to C. Grewer and by Deutsche Forschungsgemeinschaft grant GR 1393/2-2,3 awarded to C. Grewer and RA 753/1-1,2 to T. Rauen.

Lawrence G. Palmer served as editor.

Submitted: 13 July 2005
Accepted: 11 November 2005

REFERENCES

Arriza, J.L., S. Eliasof, M.P. Kavanaugh, and S.G. Amara. 1997. Excitatory amino acid transporter 5, a retinal glutamate transporter coupled to a chloride conductance. *Proc. Natl. Acad. Sci. USA*. 94: 4155–4160.

Auger, C., and D. Attwell. 2000. Fast removal of synaptic glutamate by postsynaptic transporters. *Neuron*. 28:547–558.

Bergles, D.E., J.A. Dzubay, and C.E. Jahr. 1997. Glutamate transporter currents in bergmann glial cells follow the time course of extrasynaptic glutamate. *Proc. Natl. Acad. Sci. USA*. 94:14821–14825.

Bergles, D.E., and C.E. Jahr. 1998. Glial contribution to glutamate uptake at Schaffer collateral-commissural synapses in the hippocampus. *J. Neurosci.* 18:7709–7716.

Bergles, D.E., A.V. Tzingounis, and C.E. Jahr. 2002. Comparison of coupled and uncoupled currents during glutamate uptake by GLT-1 transporters. *J. Neurosci.* 22:10153–10162.

Campiani, G., M. De Angelis, S. Armaroli, C. Fattorusso, B. Catalanotti, A. Ramunno, V. Nacci, E. Novellino, C. Grewer, D. Ionescu, et al. 2001. A rational approach to the design of selective substrates and potent nontransportable inhibitors of the excitatory amino acid transporter EAAC1 (EAAT3). New glutamate and aspartate analogues as potential neuroprotective agents. *J. Med. Chem.* 44:2507–2510.

Canepari, M., L. Nelson, G. Papageorgiou, J.E.T. Corrie, and D. Ogden. 2001. Photochemical and pharmacological evaluation of 7-nitroindolinyl-and 4-methoxy-7-nitroindolinyl-amino acids as novel, fast caged neurotransmitters. *J. Neurosci. Methods*. 112:29–42.

Conti, F., S. DeBiasi, A. Minelli, J.D. Rothstein, and M. Melone. 1998. EAAC1, a high-affinity glutamate tranporter, is localized to astrocytes and gabaergic neurons besides pyramidal cells in the rat cerebral cortex. *Cereb. Cortex*. 8:108–116.

Danbolt, N.C. 2001. Glutamate uptake. *Prog. Neurobiol.* 65:1–105.

Dehnes, Y., F.A. Chaudhry, K. Ullensvang, K.P. Lehre, J. Storm-Mathisen, and N.C. Danbolt. 1998. The glutamate transporter EAAT4 in rat cerebellar Purkinje cells: a glutamate-gated chloride channel concentrated near the synapse in parts of the dendritic membrane facing astroglia. *J. Neurosci.* 18:3606–3619.

Deitmer, J.W., A. Broer, and S. Broer. 2003. Glutamine efflux from astrocytes is mediated by multiple pathways. *J. Neurochem.* 87:127–135.

Eliasof, S., and C.E. Jahr. 1996. Retinal glial cell glutamate transporter is coupled to an anionic conductance. *Proc. Natl. Acad. Sci. USA*. 93:4153–4158.

Eliasof, S., H.B. McIlvain, R.E. Petroski, A.C. Foster, and J. Dunlop. 2001. Pharmacological characterization of threo-3-methylglutamic acid with excitatory amino acid transporters in native and recombinant systems. *J. Neurochem.* 77:550–557.

Fairman, W.A., M.S. Sonders, G.H. Murdoch, and S.G. Amara. 1998. Arachidonic acid elicits a substrate-gated proton current associated with the glutamate transporter EAAT4. *Nat. Neurosci.* 1:105–113.

Fairman, W.A., R.J. Vandenberg, J.L. Arriza, M.P. Kavanaugh, and S.G. Amara. 1995. An excitatory amino-acid transporter with properties of a ligand-gated chloride channel. *Nature*. 375:599–603.

Furuta, A., L.J. Martin, C.L. Lin, M. Dykes-Hoberg, and J.D. Rothstein. 1997. Cellular and synaptic localization of the neuronal glutamate transporters excitatory amino acid transporter 3 and 4. *Neuroscience*. 81:1031–1042.

Goldman, D.E. 1943. Potential, impedence, and rectification in membranes. *J. Gen. Physiol.* 27:37–60.

Grewer, C., S.A. Madani Mobarekeh, N. Watzke, T. Rauen, and K. Schaper. 2001. Substrate translocation kinetics of excitatory amino acid carrier 1 probed with laser-pulse photolysis of a new photolabile precursor of d-aspartic acid. *Biochemistry*. 40:232–240.

Grewer, C., and T. Rauen. 2005. Electrogenic glutamate transporters in the CNS: molecular mechanism, pre-steady-state kinetics, and their impact on synaptic signaling. *J. Membr. Biol.* 203:1–20.

Grewer, C., N. Watzke, M. Wiessner, and T. Rauen. 2000. Glutamate translocation of the neuronal glutamate transporter EAAC1 occurs within milliseconds. *Proc. Natl. Acad. Sci. USA*. 97:9706–9711.

Hodgkin, A.L., and B. Katz. 1949. The effect of sodium ions on the electrical activity of the giant axon of the squid. *J. Physiol.* 108:37–77.

Kanai, Y., and M.A. Hediger. 1992. Primary structure and functional characterization of a high-affinity glutamate transporter. *Nature*. 360:467–471.

Kanai, Y., S. Nussberger, M.F. Romero, W.F. Boron, S.C. Hebert, and M.A. Hediger. 1995. Electrogenic properties of the epithelial and neuronal high affinity glutamate transporter. *J. Biol. Chem.* 270:16561–16568.

Kugler, P., and A. Schmitt. 1999. Glutamate transporter EAAC1 is expressed in neurons and glial cells in the rat nervous system. *Glia*. 27:129–142.

Läuger, P. 1987. Voltage dependence of sodium-calcium exchange: predictions from kinetic models. *J. Membr. Biol.* 99:1–11.

Lehre, K.P., and N.C. Danbolt. 1998. The number of glutamate transporter subtype molecules at glutamatergic synapses: chemical and stereological quantification in young adult rat brain. *J. Neurosci.* 18:8751–8757.

Levy, L.M., O. Warr, and D. Attwell. 1998. Stoichiometry of the glial glutamate transporter GLT-1 expressed inducibly in a Chinese hamster ovary cell line selected for low endogenous Na^+-dependent glutamate uptake. *J. Neurosci.* 18:9620–9628.

Lin, C.-L.G., A.V. Tzingounis, L. Jin, A. Furuta, M.P. Kavanaugh, and J.D. Rothstein. 1998. Molecular cloning and expression of

the rat EAAT4 glutamate transporter subtype. *Brain Res. Mol. Brain Res.* 63:174–179.

Maier, W., J.E.T. Corrie, G. Papageorgiou, B. Laube, and C. Grewer. 2005. Comparative analysis of inhibitory effects of caged ligands for the NMDA receptor. *J. Neurosci. Methods.* 142:1–9.

Melzer, N., A. Biela, and C. Fahlke. 2003. Glutamate modifies ion conduction and voltage-dependent gating of excitatory amino Acid transporter-associated anion channels. *J. Biol. Chem.* 278: 50112–50119.

Mitrovic, A.D., F. Plesko, and R.J. Vandenberg. 2001. Zn^{2+} inhibits the anion conductance of the glutamate transporter EAAT4. *J. Biol. Chem.* 276:26071–26076.

Otis, T.S., and C.E. Jahr. 1998. Anion currents and predicted glutamate flux through a neuronal glutamate transporter. *J. Neurosci.* 18:7099–7110.

Otis, T.S., and M.P. Kavanaugh. 2000. Isolation of current components and partial reaction cycles in the glial glutamate transporter EAAT2. *J. Neurosci.* 20:2749–2757.

Picaud, S.A., H.P. Larsson, G.B. Grant, H. Lecar, and F.S. Werblin. 1995. Glutamate-gated chloride channel with glutamate-transporter-like properties in cone photoreceptors of the tiger salamander. *J. Neurophysiol.* 74:1760–1771.

Pines, G., N.C. Danbolt, M. Bjoras, Y. Zhang, A. Bendahan, L. Eide, H. Koepsell, J. Storm Mathisen, E. Seeberg, and B.I. Kanner. 1992. Cloning and expression of a rat brain l-glutamate transporter. *Nature.* 360:464–467.

Rothstein, J.D., L. Martin, A.I. Levey, M. Dykes-Hoberg, L. Jin, D. Wu, N. Nash, and R.W. Kuncl. 1994. Localization of neuronal and glial glutamate transporters. *Neuron.* 13:713–725.

Seal, R.P., Y. Shigeri, S. Eliasof, B.H. Leighton, and S.G. Amara. 2001. Sulfhydryl modification of V449C in the glutamate transporter EAAT1 abolishes substrate transport but not the substrate-gated anion conductance. *Proc. Natl. Acad. Sci. USA.* 98:15324–15329.

Shigeri, Y., K. Shimamoto, Y. Yasuda-Kamatani, R.P. Seal, N. Yumoto, T. Nakajima, and S.G. Amara. 2001. Effects of threo-β-hydroxyaspartate derivatives on excitatory amino acid transporters (EAAT4 and EAAT5). *J. Neurochem.* 79:297–302.

Sonders, M.S., and S.G. Amara. 1996. Channels in transporters. *Curr. Opin. Neurobiol.* 6:294–302.

Storck, T., S. Schulte, K. Hofmann, and W. Stoffel. 1992. Structure, expression, and functional analysis of a Na^{+}-dependent glutamate/aspartate transporter from rat brain. *Proc. Natl. Acad. Sci. USA.* 89:10955–10959.

Wadiche, J.I., and M.P. Kavanaugh. 1998. Macroscopic and microscopic properties of a cloned glutamate transporter/chloride channel. *J. Neurosci.* 18:7650–7661.

Wadiche, J.I., S.G. Amara, and M.P. Kavanaugh. 1995a. Ion fluxes associated with excitatory amino acid transport. *Neuron.* 15:721–728.

Wadiche, J.I., J.L. Arriza, S.G. Amara, and M.P. Kavanaugh. 1995b. Kinetics of a human glutamate transporter. *Neuron.* 14:1019–1027.

Watzke, N., E. Bamberg, and C. Grewer. 2001. Early intermediates in the transport cycle of the neuronal excitatory amino acid carrier EAAC1. *J. Gen. Physiol.* 117:547–562.

Zerangue, N., and M.P. Kavanaugh. 1996. Flux coupling in a neuronal glutamate transporter. *Nature.* 383:634–637.